Journal of Scientific Computing (2019) 80:1083–1115
https://doi.org/10.1007/s10915-019-00968-5

A Stabilized Semi-Implicit Euler Gauge-Invariant Method for the Time-Dependent Ginzburg–Landau Equations

Huadong Gao[1,2] · **Lili Ju**[3] · **Wen Xie**[1]

Received: 30 January 2019 / Revised: 9 March 2019 / Accepted: 24 April 2019 / Published online: 2 May 2019

Abstract

In this paper, we propose and analyze a stabilized semi-implicit Euler gauge-invariant method for numerical solution of the time-dependent Ginzburg–Landau (TDGL) equations in the two-dimensional space. The proposed method uses the well-known gauge-invariant finite difference approximations with staggered variables in a rectangular mesh, and a stabilized semi-implicit Euler discretization for time integration. The resulted fully discrete system leads to two decoupled linear systems at each time step, thus can be efficiently solved. We prove that the proposed method unconditionally preserves the point-wise boundedness of the solution and is also energy-stable. Moreover, the proposed method under the zero-electric potential gauge is shown to be equivalent to a mass-lumped version of the lowest order rectangular Nédélec edge element approximation and the Lorentz gauge scheme to a mass-lumped mixed finite element method. These indicate the method is also effective in solving the TDGL problems in non-convex domains although the solutions are often of low-regularity in such situation. Various numerical experiments are also presented to demonstrate effectiveness and robustness of the proposed method.

Keywords Time-dependent Ginzburg–Landau equations · Gauge-invariance · Staggered grid approximation · Non-convex domain · Nédélec edge element · Superconductivity

---

H. Gao's research is partially supported by National Natural Science Foundation of China under Grant Number 11871234 and Fundamental Research Funds for the Central Universities (HUST) under Grant Number 2017KFYXJJ089. L. Ju's research is partially supported by US National Science Foundation under Grant Number DMS-1818438.

✉ Huadong Gao
huadong@hust.edu.cn

Lili Ju
ju@math.sc.edu

Wen Xie
wenxie_@hust.edu.cn

[1] School of Mathematics and Statistics, Huazhong University of Science and Technology, Wuhan 430074, People's Republic of China

[2] Hubei Key Laboratory of Engineering Modeling and Scientific Computing, Huazhong University of Science and Technology, Wuhan 430074, People's Republic of China

[3] Department of Mathematics, University of South Carolina, Columbia, SC 29208, USA

1 Introduction

The governing equations for type-II superconductors in an external magnetic field are the following time-dependent Ginzburg–Landau (TDGL) equations:

$$\frac{\partial \psi}{\partial t} + i\kappa\Phi\psi + \left(\frac{i}{\kappa}\nabla + \mathbf{A}\right)^2 \psi + (|\psi|^2 - 1)\psi = 0\,, \qquad \text{in } \Omega \times (0, T], \quad (1.1)$$

$$\frac{\partial \mathbf{A}}{\partial t} + \nabla\Phi + \mathbf{curl}\,\mathrm{curl}\,\mathbf{A} + \mathrm{Re}\left[\psi^*\left(\frac{i}{\kappa}\nabla\psi + \mathbf{A}\psi\right)\right] = \mathbf{curl}\,H, \quad \text{in } \Omega \times (0, T], \quad (1.2)$$

with the boundary and initial conditions as

$$\left(\frac{i}{\kappa}\nabla\psi + \mathbf{A}\right)\cdot\mathbf{n} = 0, \quad \mathrm{curl}\,\mathbf{A} = H, \quad \left(\frac{\partial \mathbf{A}}{\partial t} + \nabla\Phi\right)\cdot\mathbf{n} = 0, \quad \text{on } \partial\Omega \times [0, T], \quad (1.3)$$

$$\psi(\mathbf{x}, 0) = \psi_0(\mathbf{x}), \quad \mathbf{A}(\mathbf{x}, 0) = \mathbf{A}_0(\mathbf{x}), \qquad \text{in } \Omega. \quad (1.4)$$

where Ω is a bounded domain in $\mathbb{R}^2$, $\mathbf{n}$ is the unit outer normal vector to $\partial\Omega$, κ is the Ginzburg–Landau parameter, the unknown ψ is a scalar complex function which denotes the order parameter and ψ^* denotes its conjugate, the real vector unknown $\mathbf{A}$ is the magnetic potential, Φ is the electric potential, and H stands for a constant external applied magnetic field. Here, $\mathrm{Re}[\cdot]$ denotes the real part of the content in bracket. In this model, $|\psi| = 1$ corresponds to the superconducting state and $|\psi| = 0$ denotes the normal state, while $0 < |\psi| < 1$ stands for the mixed (or vortex) state. For a vector function $\boldsymbol{u} = [u_1, u_2]^T$ and scalar function f, the standard calculus operators in the two dimensional space in (1.1)–(1.4) are defined as follows:

$$\mathrm{div}\,\boldsymbol{u} = \frac{\partial u_1}{\partial x} + \frac{\partial u_2}{\partial y}, \quad \nabla f = \left[\frac{\partial f}{\partial x}, \frac{\partial f}{\partial y}\right]^T, \quad \mathrm{curl}\,\boldsymbol{u} = \frac{\partial u_2}{\partial x} - \frac{\partial u_1}{\partial y}, \quad \mathbf{curl}\,f = \left[\frac{\partial f}{\partial y}, -\frac{\partial f}{\partial x}\right]^T.$$

The above TDGL system was first deduced by Gorkov and Eliashberg [20] from the microscopic Bardeen–Cooper–Schrieffer theory. We refer to [5,12,37] for more discussion on the superconductivity model. One of the most important issues in superconductivity is to investigate the vortex motion. To obtain the correct vortex pattern, it is crucial to make sure that the key physical quantities are conserved, and relevant physical principles are retained at the discrete level. There have been tremendous numerical methods for the TDGL equations (1.1)–(1.4). For conventional finite difference methods, we refer to [29,34] and reference therein; for finite element methods, we refer to [4,6,7,10,12,16–19,25–28,31–33]. However, none of the numerical methods mentioned above can preserve the point-wise boundedness in the discrete sense, $|\psi_h| \leq 1$ (a property satisfied by the exact solution ψ). Motivated by this, gauge-invariant schemes have been developed and widely used in practice, which can preserve the point-wise boundedness. One of the typical examples is the gauge-invariant finite difference method, see [3,9,11,15,21–24,35] for its analysis and applications. We shall also mention that a co-volume approximation for the steady state GL equation had been studied in [14]. The first rigorous analysis of the gauge-invariant schemes was done in [11] for a rectangular domain with a uniform mesh partition, in which a fully nonlinear backward Euler gauge-invariant scheme was studied and the point-wise boundedness and stability of the scheme were proved under certain conditions. In particular, under the assumption that the exact solution $(\psi, \mathbf{A})$ is sufficiently smooth, a priori error estimate for the gauge-invariant scheme under Lorentz gauge was derived there. However, it is well-known that the **curl** curl operator in (1.2) will introduce strong singularities near the re-entrant corner region for non-convex domains [27]. Thus, it also remains an interesting question whether the gauge-invariant schemes are still feasible for non-convex domains.

In this paper, we propose a stabilized semi-implicit Euler gauge-invariant scheme for the TDGL Eqs. (1.1)–(1.4). At each time step, the proposed scheme only needs to solve two linear systems, and thus dramatically reduces the computational cost compared to the solution of a coupled nonlinear system required by the classic fully nonlinear approach proposed in [11]. Moreover, the proposed scheme unconditionally preserves the point-wise boundedness of ψ and also satisfies the energy stability property under a very relaxed condition. Extensive numerical experiments are also tested to investigate the performance of the proposed scheme. We use the proposed method to study the vortex pattern in non-convex superconductors, which has many applications in industry [1]. More importantly, it is shown in this paper that the proposed scheme under the zero electric potential gauge is equivalent to a mass-lumped version of the lowest order rectangular Nédélec edge-element approximation; and the scheme under Lorentz gauge can be viewed as a mass-lumped version of a mixed finite element method. For the non-convex polygon, the exact solution $\mathbf{A}$ in the TDGL equations only belongs to $\mathbf{H}^s(\Omega)$ for $\frac{1}{2} < s < 1$. It is well-known that the $\mathbf{H}(\mathbf{curl})$ conforming Nédélec edge element can solve for the **curl curl** problem correctly on non-convex geometries, which has attracted much attention and been successfully used for simulating electromagnetics. Thus, the equivalence of these two approximations implies that the proposed schemes could also effectively solve the TDGL equations on non-convex domains.

This paper is organized as follows. In Sect. 2, we propose the stabilized semi-implicit Euler gauge-invariant scheme for solving the TDGL equations and its forms under the zero-electric potential gauge and the Lorentz gauge respectively. In Sect. 3, we prove that the proposed scheme satisfies the point-wise boundedness unconditionally and the energy stability. Their equivalences to the lowest order rectangular Nédélec edge finite element approximation and a mass-lumped mixed finite element method respectively are discussed in Sect. 4. In Sect. 5, various numerical examples on convex and non-convex domains are presented and the results demonstrate that the proposed schemes are effective and provides correct vortex patterns for superconductors in all cases. Some concluding remarks are finally given in Sect. 6.

2 A Stabilized Semi-Implicit Euler Gauge-Invariant Method for the TDGL Equations

2.1 Preliminaries

For simplicity and clarity of exposition, let us take a uniform time partition $\{t_n = n\Delta t\}_{n=0}^{N}$ with $\Delta t = \frac{T}{N}$ together with a uniform rectangular mesh Γ_h of size h for the two-dimensional domain Ω. Follow the notations defined in [11], assume that for the mesh Γ_h, there are N_0 nodes $\{\boldsymbol{x}_j\}$, N_1 edges $\{s_{jk}\}$ where s_{jk} connects $\boldsymbol{x}_j$ and $\boldsymbol{x}_k$, and N_2 cells $\{\tau_{jklm}\}$ which has four counterclockwise labeled nodes $\boldsymbol{x}_j$, $\boldsymbol{x}_k$, $\boldsymbol{x}_l$ and $\boldsymbol{x}_m$. The center of the cell τ_{jklm} is denoted by $\boldsymbol{x}_{jklm}$. From the original mesh Γ_h, we can obtain a dual mesh Γ_h' by shifting each cell $\frac{h}{2}$ (see Fig. 1). The cell in Γ_h' containing $\boldsymbol{x}_j$ is denoted by τ_j' with area $|\tau_j'|$. Let h_{jk}' be the length of the edge in Γ_h' that bisects s_{jk}. It is easy to see that $h_{jk}' = h$ in the interior domain while $h_{jk}' = \frac{h}{2}$ on the boundary. Consequently, $|\tau_j'|$ will take one of the four values $\{h^2, \frac{3h^2}{4}, \frac{h^2}{2}, \frac{h^2}{4}\}$, see Fig. 1 for each case.

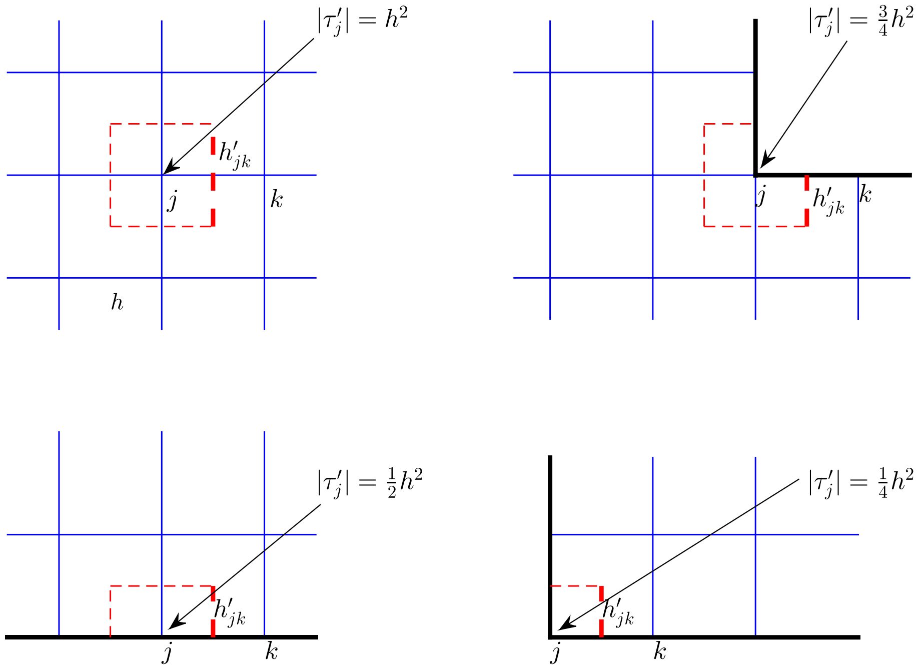

Fig. 1 An illustration of the rectangular mesh and its duality

Next we shall define some discrete norms. For a vector $\overrightarrow{v} \in U = \mathbb{R}^{N_0}$ with the component v_j corresponding to the vertex $\boldsymbol{x}_j$, define the discrete L^p norm on U by

$$\|\overrightarrow{v}\|_{U,p} = \Big(\sum_j |v_j|^p|\tau_j'|\Big)^{1/p}, \quad 1 \le p < \infty, \qquad \text{and} \qquad \|\overrightarrow{v}\|_{U,\infty} = \max_j |v_j|.$$

Here $\sum_j$ denotes the sum over all possible index j. Moreover, define $\langle\cdot,\cdot\rangle_U$ to be the inner product which yields the natural norm $\|\cdot\|_{U,2}$. For a vector field $\overrightarrow{f}$ defined by its value f_{jklm} at the center of each primal cell τ_{jklm}, we use the convention that $f_{jklm} = -f_{mlkj}$ if the vertices are labeled clockwise and denote the set of all vectors with this convention by V, where V is a vector space isomorphic to $\mathbb{R}^{N_2}$. Define the discrete L^p norm on V by

$$\|\overrightarrow{f}\|_{V,p} = \Big(\sum_{jklm} |f_{jklm}|^p|\tau_{jklm}|\Big)^{1/p}, \quad 1 \le p < \infty, \qquad \text{and} \qquad \|\overrightarrow{f}\|_{V,\infty} = \max_{jklm} |f_{jklm}|.$$

For a vector field $\overrightarrow{A}$ defined at the midpoint $\boldsymbol{x}_{jk} = \frac{\boldsymbol{x}_j+\boldsymbol{x}_k}{2}$ of each edge s_{jk}, its component a_{jk} denotes a vector $a_{jk}\mathbf{t}_{jk}$ where $\mathbf{t}_{jk}$ is a unit vector in the direction $\boldsymbol{x}_j \to \boldsymbol{x}_k$. We also use the convention that $a_{jk} = -a_{kj}$. Then, $\{a_{jk}\}$ constitute a space W which is isomorphic to $\mathbb{R}^{N_1}$. Define the discrete L^p norm on W by

$$\|\overrightarrow{A}\|_{W,p} = \Big(\sum_{jk} |a_{jk}|^p h\, h_{jk}'\Big)^{1/p}, \quad 1 \le p < \infty, \qquad \text{and} \qquad \|\overrightarrow{A}\|_{W,\infty} = \max_{jk} |a_{jk}|.$$

Table 1 The staggered discrete variables

Physical variables	Notations	Location on the mesh
Order parameter	$\overrightarrow{\psi}^n$	Vertices $\{\boldsymbol{x}_j\}$
Electric potential	$\overrightarrow{\Phi}^n$	Vertices $\{\boldsymbol{x}_j\}$
Magnetic potential	$\overrightarrow{A}^n$	Midpoints of edges $\{s_{jk}\}$
Induced magnetic field	$\overrightarrow{c}^n$	Center of cells $\{\boldsymbol{x}_{jklm}\}$
External applied magnetic field	$\overrightarrow{H}$	Center of cells $\{\boldsymbol{x}_{jklm}\}$

Now, we define some discrete operators which will be frequently used in the rest part of the paper. As the discrete variables are staggered on nodes, edges and cells, we list in Table 1 the variables and their locations on the mesh.

For $\overrightarrow{u} \in U$, we define $\overrightarrow{w} = \nabla_h \overrightarrow{u} \in W$ by

$$w_{jk} = (\nabla_h \overrightarrow{u})_{jk} = \frac{u_k - u_j}{h} \tag{2.1}$$

on each edge s_{jk}, where ∇_h is the gradient matrix. For $\overrightarrow{g} \in V$, we introduce a matrix $\nabla_h^\perp$ and define $\overrightarrow{w} = \nabla_h^\perp \overrightarrow{g} \in W$ by

$$w_{jk} = (\nabla_h^\perp \overrightarrow{g})_{jk} = \frac{g_{jklm} - g_{jkl'm'}}{h'_{jk}} \tag{2.2}$$

on the common edge s_{jk} of two neighboring cells τ_{jklm} and $\tau_{jkl'm'}$. If s_{jk} lies on the boundary, we define

$$w_{jk} = (\nabla_h^\perp \overrightarrow{g})_{jk} = \frac{g_{jklm}}{h'_{jk}} . \tag{2.3}$$

Let $\overrightarrow{A} \in W$ be a vector field defined at the midpoint of each edge. The circulation in the cell τ_{jklm} with four vertices $\boldsymbol{x}_j, \boldsymbol{x}_k, \boldsymbol{x}_l$ and $\boldsymbol{x}_m$ is given by

$$c_{jklm} := \frac{a_{jk} + a_{kl} + a_{lm} + a_{mj}}{h},$$

which can be rewritten in matrix form

$$C_h \overrightarrow{A} = \overrightarrow{c}, \tag{2.4}$$

where C_h might be viewed as an approximation of the curl operator. We approximate the divergence on each dual cell τ'_j containing the vertex $\boldsymbol{x}_j$ by

$$d_j := \frac{1}{|\tau'_j|} \sum_{k \to j} a_{jk}\, h'_{jk} ,$$

which can be rewritten in the matrix form

$$D_h \overrightarrow{A} = \overrightarrow{d}, \tag{2.5}$$

where D_h could be viewed as an approximation of the operator div. The following lemma provide a discrete version of integration by parts formulas and the orthogonality of vector fields.

Lemma 2.1 *Let* $\overrightarrow{u} \in W$, D_h, C_h *be matrices defined as in* (2.4), (2.5), *and* ∇_h, $\nabla_h^\perp$ *as defined in* (2.1), (2.2)–(2.3). *Then*

$$\left\langle D_h \overrightarrow{u}\,,\, \overrightarrow{f} \right\rangle_U = -\left\langle \overrightarrow{u}\,,\, \nabla_h \overrightarrow{f} \right\rangle_W, \quad \forall \overrightarrow{f} \in U \tag{2.6}$$

$$\left\langle C_h \overrightarrow{u}\,,\, \overrightarrow{g} \right\rangle_V = \left\langle \overrightarrow{u}\,,\, \nabla_h^\perp \overrightarrow{g} \right\rangle_W, \quad \forall \overrightarrow{g} \in V \tag{2.7}$$

$$C_h \nabla_h \overrightarrow{f} = \overrightarrow{0}\,, \quad \forall \overrightarrow{f} \in U \quad \textit{and} \quad D_h \nabla_h^\perp \overrightarrow{g} = \overrightarrow{0}\,, \quad \forall \overrightarrow{g} \in V. \tag{2.8}$$

In the continuous setting, the Ginzburg–Landau energy functional is defined by

$$\mathcal{G}(\psi, A) = \int_\Omega \left(\frac{1}{2} \left| \left(\frac{i}{\kappa} \nabla + \mathbf{A} \right) \psi \right|^2 + \frac{1}{4} \left(1 - |\psi|^2 \right)^2 + \frac{1}{2} \left| \mathrm{curl} \mathbf{A} - H \right|^2 \right) \mathrm{d}\boldsymbol{x}\,. \tag{2.9}$$

Then, with the above notations, its corresponding discrete version can be written into the following form

$$\begin{aligned} \mathcal{G}^h(\overrightarrow{\psi}\,, \overrightarrow{A}\,) = {} & \frac{1}{2} \sum_{jk} \frac{h h'_{jk}}{\kappa^2} \left| \frac{\psi_k \exp(-i\kappa a_{jk} h) - \psi_j}{h} \right|^2 + \sum_j \frac{|\tau'_j|}{4} (1 - |\psi_j|^2)^2 \\ & + \frac{1}{2} \sum_{jklm} \left(a_{jk} + a_{kl} + a_{lm} + a_{mj} - H_{jklm} h \right)^2 . \end{aligned} \tag{2.10}$$

2.2 A Stabilized Semi-Implicit Euler Gauge-Invariant Method

Based on the above notations, we present a stabilized semi-implicit Euler gauge-invariant method for the time-space discretization of the TDGL Eqs. (1.1)–(1.4) as follows: for $n = 1, \ldots, N$, solve

$$\begin{aligned} & \frac{\psi_j^n - \psi_j^{n-1} \exp(-i\kappa \Phi_j^n \Delta t)}{\Delta t} + \frac{1}{|\tau'_j|} \sum_{k \to j} \frac{h'_{jk}}{\kappa^2} \left(\frac{\psi_j^n - \psi_k^n \exp(-i\kappa a_{jk}^n h)}{h} \right) \\ & + \alpha \left(\psi_j^n - \psi_j^{n-1} \exp(-i\kappa \Phi_j^n \Delta t) \right) + (|\psi_j^{n-1}|^2 - 1) \psi_j^n = 0\,, \end{aligned} \tag{2.11}$$

$$\frac{a_{jk}^n - a_{jk}^{n-1}}{\Delta t} + \frac{\Phi_k^n - \Phi_j^n}{h} + \left(\nabla_h^\perp (\overrightarrow{c}^{\,n} - \overrightarrow{H}) \right)_{jk} = \frac{1}{h\,\kappa} \mathrm{Re} \left[i (\psi_k^{n-1})^* \psi_j^{n-1} \exp(i\kappa a_{jk}^{n-1} h) \right], \tag{2.12}$$

with $\overrightarrow{c}^{\,n} = C_h \overrightarrow{A}^{\,n}$, where $\alpha > 0$ is a stabilizing parameter, and the initial condition for ψ is taken to be

$$\psi^0 = \{\psi_0(\boldsymbol{x}_j)\}, \tag{2.13}$$

and an initial $\overrightarrow{A}^{\,0}$ such that

$$C_h \overrightarrow{A}^{\,0} = \overrightarrow{c}\,(0) \in V, \quad D_h \overrightarrow{A}^{\,0} = \overrightarrow{0} \in U, \tag{2.14}$$

where $\overrightarrow{c}\,(0)$ on cell τ_{jklm} is defined as $c_{jklm}(0) = \frac{1}{|\tau_{jklm}|} \int_{\tau_{jklm}} \mathrm{curl} \mathbf{A}_0 \, \mathrm{d}\boldsymbol{x}$.

Here we propose to use the popular stabilization technique for solving ψ. That is, a term $\alpha\left(\psi_j^n - \psi_j^{n-1} \exp(-i\kappa \Phi_j^n \Delta t)\right)$ is added in the scheme (2.11) for ψ_j^n. We will show in Sect. 3.1 that the above scheme (2.11)–(2.12) preserves $|\psi_j^n| \le 1$ unconditionally, i.e., for any

$\Delta t > 0$. We refer to [13,38] for more discussion on the stabilization technique for phase field equations. Fully decoupled schemes can be obtained by linearizing more nonlinear terms. For instance, using $(|\psi_j^{n-1}|^2 - 1)\psi_j^{n-1}$ in (2.11) at t_n gives another semi-implicit scheme. However, the proposed scheme (2.11)–(2.12) preserves a discrete gauge-invariant property, which is a crucial feature of the original TDGL Eqs. (1.1)–(1.2).

Remark 2.2 The TDGL Eqs. (1.1)–(1.4) enjoy a gauge-invariant property, namely, if $(\psi, \mathbf{A}, \Phi)$ is a solution to (1.1)–(1.4), then for any given real scalar function $f(\boldsymbol{x}, t)$ satisfying $f(\boldsymbol{x}, 0) = 0$, the transformation

$$\mathcal{G}_f \,:\, (\psi,\ \mathbf{A},\ \Phi) \longmapsto \left(\psi e^{i\kappa f},\ \mathbf{A} + \nabla f,\ \Phi - \frac{\partial f}{\partial t}\right) \tag{2.15}$$

provides a more general solution $(\psi e^{i\kappa f}, \mathbf{A} + \nabla f, \Phi - \frac{\partial f}{\partial t})$ for (1.1)–(1.4). The physical quantities are invariant under the above gauge transformation, i.e., the density of superconducting pairs $|\psi e^{i\kappa f}| = |\psi|$ and the magnetic field $\operatorname{curl}(\mathbf{A} + \nabla f) = \operatorname{curl} \mathbf{A}$. The proposed scheme (2.11)–(2.12) preserves a discrete gauge-invariant property. Given $\overrightarrow{f} \in [R^{N_0}]^N$, with $f_j^0 = 0$ for any j, We define

$$\mathcal{T}_f^h(\overrightarrow{\psi}, \overrightarrow{A}, \overrightarrow{\Phi}) = (\overrightarrow{\zeta}, \overrightarrow{Q}, \overrightarrow{\Theta}) \tag{2.16}$$

where

$$\zeta_j^n = \psi_j^n \exp(i\kappa f_j^n), \quad \Theta_j^n = \Phi_j^n - \frac{f_j^n - f_j^{n-1}}{\Delta t}, \quad q_{jk}^n = a_{jk}^n + \frac{f_k^n - f_j^n}{h}. \tag{2.17}$$

If $(\overrightarrow{\psi}, \overrightarrow{A}, \overrightarrow{\Phi})$ is a solution of the numerical method (2.11)–(2.12), then so is $\mathcal{T}_f^h(\overrightarrow{\psi}, \overrightarrow{A}, \overrightarrow{\Phi})$.

2.2.1 Under the Zero-Electric Potential Gauge

By imposing

$$\Phi - \frac{\partial f}{\partial t} = 0, \quad \text{with} \quad f\big|_{t=0} = 0, \tag{2.18}$$

the TDGL Eqs. (1.1)–(1.4) under the zero-electric potential gauge become

$$\frac{\partial \psi}{\partial t} + \left(\frac{i}{\kappa}\nabla + \mathbf{A}\right)^2 \psi + (|\psi|^2 - 1)\psi = 0, \qquad \text{in } \Omega \times (0, T], \tag{2.19}$$

$$\frac{\partial \mathbf{A}}{\partial t} + \mathbf{curl}\operatorname{curl}\mathbf{A} + \operatorname{Re}\left[\psi^*\left(\frac{i}{\kappa}\nabla\psi + \mathbf{A}\psi\right)\right] = \mathbf{curl}\, H, \qquad \text{in } \Omega \times (0, T], \tag{2.20}$$

with the boundary and initial conditions

$$\frac{\partial \psi}{\partial \mathbf{n}} = 0, \quad \mathbf{A} \cdot \mathbf{n} = 0, \quad \operatorname{curl}\mathbf{A} = H, \qquad \text{on } \partial\Omega \times [0, T], \tag{2.21}$$

$$\psi(x, 0) = \psi_0(x), \quad \mathbf{A}(x, 0) = \mathbf{A}_0(x), \qquad \text{in } \Omega. \tag{2.22}$$

Similar to (2.18), by setting

$$\frac{f_j^n - f_j^{n-1}}{\Delta t} = \Phi_j^n, \quad \text{with} \quad f_j^0 = 0, \tag{2.23}$$

in the proposed scheme (2.11)–(2.12), we obtain the following stabilized semi-implicit zero-electric potential gauge scheme for solving the TDGL Eqs. (2.19)–(2.20):

$$\begin{aligned}&\frac{\psi_j^n - \psi_j^{n-1}}{\Delta t} + \frac{1}{|\tau_j'|}\sum_{k\to j}\frac{h'_{jk}}{\kappa^2}\Big(\frac{\psi_j^n - \psi_k^n \exp(-i\kappa a_{jk}^n h)}{h}\Big) + \alpha\,(\psi_j^n - \psi_j^{n-1})\\ &\quad + (|\psi_j^{n-1}|^2 - 1)\,\psi_j^n = 0\,,\end{aligned} \tag{2.24}$$

$$\frac{a_{jk}^n - a_{jk}^{n-1}}{\Delta t} + \big(\nabla_h^\perp(\overrightarrow{c}^{\,n} - \overrightarrow{H})\big)_{jk} = \frac{1}{h\,\kappa}\mathrm{Re}\Big[i\,(\psi_k^{n-1})^*\psi_j^{n-1}\exp(i\kappa a_{jk}^{n-1}h)\Big]. \tag{2.25}$$

It should be noted that the above system of (2.24)–(2.25) is decoupled and linear. At each time step, for given $(\overrightarrow{\psi}^{\,n-1}, \overrightarrow{A}^{\,n-1})$, one shall first solve for $\overrightarrow{A}^{\,n}$ from (2.25), and then compute $\overrightarrow{\psi}^{\,n}$ from (2.24). The linear system (2.25) for $\{a_{jk}\}$ can be rewritten into the matrix form

$$\frac{1}{\Delta t}\overrightarrow{A}^{\,n} + \mathbf{K}_1\overrightarrow{A}^{\,n} = \frac{1}{\Delta t}\overrightarrow{A}^{\,n-1} + \mathbf{E}_1\overrightarrow{H} + \overrightarrow{N}(\overrightarrow{\psi}^{\,n-1}, \overrightarrow{A}^{\,n-1}), \tag{2.26}$$

where $\mathbf{K}_1$ denotes the coefficient matrix derived from the following expression

$$\frac{1}{h\,h'_{jk}}\frac{\partial}{\partial a_{jk}^n}\Big\{\frac{1}{2}\sum_{jklm}\big(a_{jk}^n + a_{kl}^n + a_{lm}^n + a_{mj}^n - H_{jklm}h\big)^2\Big\} \quad\Longrightarrow\quad \mathbf{K}_1\overrightarrow{A}^{\,n}, \tag{2.27}$$

$\mathbf{E}_1$ is the matrix generated by $\nabla_h^\perp$, and $\overrightarrow{N}(\overrightarrow{\psi}^{\,n-1}, \overrightarrow{A}^{\,n-1})$ denotes the remaining nonlinear term.

2.2.2 Under the Lorentz Gauge

By requiring

$$\begin{cases}\frac{\partial f}{\partial t} - \Delta f = \Phi + \operatorname{div}\mathbf{A}, & \text{in } \Omega\times[0,T],\\ \frac{\partial f}{\partial \mathbf{n}} = -\mathbf{A}\cdot\mathbf{n}, & \text{on } \partial\Omega\times[0,T],\\ f(\boldsymbol{x},0) = 0, & \text{in } \Omega,\end{cases}$$

the TDGL Eqs. (1.1)–(1.4) under the Lorentz gauge become

$$\frac{\partial\psi}{\partial t} - i\kappa(\operatorname{div}\mathbf{A})\psi + \Big(\frac{i}{\kappa}\nabla + \mathbf{A}\Big)^2\psi + (|\psi|^2-1)\psi = 0\,, \qquad \text{in } \Omega\times(0,T], \tag{2.28}$$

$$\frac{\partial\mathbf{A}}{\partial t} - \nabla\operatorname{div}\mathbf{A} + \mathbf{curl}\,\operatorname{curl}\mathbf{A} + \mathrm{Re}\Big[\psi^*\Big(\frac{i}{\kappa}\nabla\psi + \mathbf{A}\psi\Big)\Big] = \mathbf{curl}\,H, \qquad \text{in } \Omega\times(0,T], \tag{2.29}$$

with the following boundary and initial conditions

$$\frac{\partial\psi}{\partial\mathbf{n}} = 0, \quad \mathbf{A}\cdot\mathbf{n} = 0, \quad \operatorname{curl}\mathbf{A} = H \qquad \text{on } \partial\Omega\times[0,T], \tag{2.30}$$

$$\psi(x,0) = \psi_0(x), \quad \mathbf{A}(x,0) = \mathbf{A}_0(x), \qquad \text{in } \Omega. \tag{2.31}$$

Correspondingly, for the discrete variables, we impose

$$\Phi_j^n = -\frac{1}{|\tau_j'|}\Big(\sum_{k\to j}a_{jk}^n h'_{jk}\Big) = -d_j^n$$

where $\overrightarrow{f}^0 = \overrightarrow{0}$ and

$$\frac{f_j^n - f_j^{n-1}}{\Delta t} - \frac{1}{|\tau_j'|}\sum_{k\to j}\frac{f_k^n - f_j^n}{h_{kj}}h'_{kj} = \Phi_j^n + d_j^n\,, \tag{2.32}$$

which results in the following stabilized semi-implicit Lorentz gauge scheme for solving the TDGL Eqs. (2.28)–(2.29):

$$\frac{\psi_j^n - \psi_j^{n-1}\exp(i\kappa d_j^n\Delta t)}{\Delta t} + \frac{1}{|\tau_j'|}\sum_{k\to j}\frac{h'_{jk}}{\kappa^2}\Big(\frac{\psi_j^n - \psi_k^n\exp(-i\kappa a_{jk}^n h)}{h}\Big)$$

$$+\,\alpha\,(\psi_j^n - \psi_j^{n-1}\exp(i\kappa d_j^n\Delta t)) + (|\psi_j^{n-1}|^2 - 1)\psi_j^n = 0\,, \tag{2.33}$$

$$\frac{a_{jk}^n - a_{jk}^{n-1}}{\Delta t} + \left(\nabla_h\overrightarrow{\Phi}^n\right)_{jk} + \left(\nabla_h^{\perp}(\overrightarrow{c}^n - \overrightarrow{H})\right)_{jk} = \frac{1}{h\,\kappa}\mathrm{Re}\left[i(\psi_k^{n-1})^*\psi_j^{n-1}\exp(i\kappa a_{jk}^{n-1}h)\right], \tag{2.34}$$

with $\overrightarrow{\Phi}^n = -D_h\overrightarrow{A}^n = -\overrightarrow{d}^n$. The initial condition (2.13)–(2.14) can also be used here.

It is easy to see that the above system of (2.33)–(2.34) is again decoupled and linear. At each time step, for given $(\overrightarrow{\psi}^{n-1}, \overrightarrow{A}^{n-1})$, one shall first solve for $\overrightarrow{A}^n$ from (2.34) and then compute $\overrightarrow{\psi}^n$ from (2.33).

Remark 2.3 We note that a fully implicit backward Euler Lorentz gauge scheme was first studied by Du [11], where a point-wise bound and energy stability of the scheme were derived. Moreover, a priori error estimate was also obtained under a strong regularity assumption in [11].

3 Stability Analysis

3.1 Unconditional Point-Wise Boundedness

We below show that the proposed semi-implicit Euler gauge-invariant scheme (2.11)–(2.12) is unconditionally point-wise bounded when the stabilizing parameter $\alpha \geq 2$.

Theorem 3.1 *Let $(\overrightarrow{\psi}^n, \overrightarrow{A}^n)$ be the solution of the stabilized semi-implicit Euler gauge invariant scheme (2.11)–(2.12) and assume that the stabilizing parameter $\alpha \geq 2$. If $|\psi_0(\boldsymbol{x})| \leq 1$, then for any $\Delta t > 0$ it holds*

$$\|\overrightarrow{\psi}^n\|_{U,\infty} \leq 1$$

for all $n \geq 0$.

Proof It is easy to verify that $\|\overrightarrow{\psi}^0\|_{U,\infty} \leq 1$ at the initial time step t_0. We will prove Theorem 3.1 by mathematical induction. Assume that $\|\overrightarrow{\psi}^m\|_{U,\infty} \leq 1$ holds for index $m = 0, 1, \ldots, n-1$. We shall prove $\|\overrightarrow{\psi}^n\|_{U,\infty} \leq 1$ also holds.

The scheme (2.11) can be rewritten into

$$\Big(1+\Delta t(\alpha+|\psi_j^{n-1}|^2-1)\Big)\,\psi_j^n+\frac{\Delta t}{|\tau_j'|}\sum_{k\to j}\frac{h'_{jk}}{\kappa^2}\left(\frac{\psi_j^n-\psi_k^n\exp(-i\kappa a_{jk}^n h)}{h}\right)$$
$$=(1+\Delta t\alpha)\psi_j^{n-1}\exp(-i\kappa\Phi_j^n\Delta t)\,.$$

Let j_0 be the index such that $|\psi_{j_0}^n|=\max_j|\psi_j^n|$. Then, at $\boldsymbol{x}_{j_0}$, multiplying the above equation by $(\psi_{j_0}^n)^*$ gives

$$\Big(1+\Delta t(\alpha+|\psi_{j_0}^{n-1}|^2-1)\Big)\,|\psi_{j_0}^n|^2=-\frac{\Delta t}{|\tau_{j_0}'|}\sum_{k\to j_0}\frac{h'_{j_0k}}{\kappa^2}\left(\frac{|\psi_{j_0}^n|^2-(\psi_{j_0}^n)^*\psi_k^n\exp(-i\kappa a_{j_0k}^n h)}{h}\right)$$
$$+(1+\Delta t\alpha)(\psi_{j_0}^n)^*\psi_{j_0}^{n-1}\exp(-i\kappa\Phi_{j_0}^n\Delta t),$$

which further leads to the following inequality

$$\begin{aligned}\Big(1+\Delta t(\alpha+|\psi_{j_0}^{n-1}|^2-1)\Big)\,|\psi_{j_0}^n|^2&\le\frac{\Delta t}{|\tau_{j_0}'|}\sum_{k\to j_0}\frac{h'_{j_0k}}{\kappa^2}\left(\frac{|\psi_{j_0}^n||\psi_k^n|-|\psi_{j_0}^n|^2)}{h}\right)\\&\quad+(1+\Delta t\alpha)|\psi_{j_0}^n||\psi_{j_0}^{n-1}|\\&\le(1+\Delta t\alpha)|\psi_{j_0}^n||\psi_{j_0}^{n-1}|.\end{aligned}\tag{3.1}$$

The above estimate (3.1) then yields

$$|\psi_{j_0}^n|^2\le\frac{(1+\Delta t\alpha)|\psi_{j_0}^n||\psi_{j_0}^{n-1}|}{1+\Delta t(\alpha+|\psi_j^{n-1}|^2-1)}.\tag{3.2}$$

If $|\psi_{j_0}^n|=0$, the bound $|\psi_{j_0}^n|\le 1$ naturally holds. If $|\psi_{j_0}^n|\ne 0$, denote $1\ge\beta=1-|\psi_{j_0}^{n-1}|\ge 0$ and the inequality (3.2) gives us

$$\begin{aligned}|\psi_{j_0}^n|&\le\frac{(1+\Delta t\alpha)|\psi_{j_0}^{n-1}|}{1+\Delta t(\alpha+|\psi_j^{n-1}|^2-1)}=\frac{(1+\Delta t\alpha)(1-\beta)}{1+\Delta t(\alpha+(1-\beta)^2-1)}\\&=\frac{(1+\Delta t\alpha)-(1+\Delta t\alpha)\beta}{(1+\Delta t\alpha)-(2-\beta)\Delta t\beta}=\frac{(1+\Delta t\alpha)-(\frac{1}{\Delta t}+\alpha)\Delta t\beta}{(1+\Delta t\alpha)-(2-\beta)\Delta t\beta}\le 1\,,\end{aligned}$$

where we have used the fact that $\alpha\ge 2$. The proof is then completed. □

Thus in the remaining part of the paper, we always assume $\alpha\ge 2$.

3.2 Energy Stability

In this subsection, we establish the energy stability for the stabilized semi-implicit zero-electric potential gauge scheme (2.24)–(2.25).

Theorem 3.2 *Let $(\overrightarrow{\psi}^n,\overrightarrow{A}^n)$ be the solution of the stabilized semi-implicit zero-electric potential gauge (2.24)–(2.25). Then, there exists a positive constant C independent of h, Δt and the stabilizing parameter α, such that for any $\Delta t<1/4$*

$$\mathcal{G}^h(\overrightarrow{\psi}^n,\overrightarrow{A}^n)\le C\mathcal{G}^h(\overrightarrow{\psi}^0,\overrightarrow{A}^0)\,.\tag{3.3}$$

Proof Multiplying (2.24)–(2.25) by $|\tau_j'|(\psi_j^n-\psi_j^{n-1})^*$ and $hh'_{jk}(a_{jk}^n-a_{jk}^{n-1})$, respectively, and then summing up the resulting equations, we have

$$\begin{aligned}
&\sum_j|\tau_j'|\frac{|\psi_j^n-\psi_j^{n-1}|^2}{\Delta t}+\sum_j\sum_{k\to j}\frac{h'_{jk}}{\kappa^2}\left(\frac{\psi_j^n-\psi_k^n\exp(-i\kappa a_{jk}^n h)}{h}\right)(\psi_j^n-\psi_j^{n-1})^*\\
&\quad+\sum_j|\tau_j'|\big(\alpha(\psi_j^n-\psi_j^{n-1})+(|\psi_j^{n-1}|^2-1)\psi_j^n\big)(\psi_j^n-\psi_j^{n-1})^*+\sum_{jk}hh'_{jk}\frac{|a_{jk}^n-a_{jk}^{n-1}|^2}{\Delta t}\\
&\quad+\sum_{jk}hh'_{jk}\left(\nabla^\perp\overrightarrow{c}^{\,n}-\overrightarrow{H}\right)_{jk}(a_{jk}^n-a_{jk}^{n-1})\\
&=\sum_{jk}hh'_{jk}\mathrm{Re}\left[\frac{i}{h\kappa}(\psi_k^{n-1})^*\psi_j^{n-1}\exp(i\kappa a_{jk}^{n-1}h)\right](a_{jk}^n-a_{jk}^{n-1})\,. \qquad (3.4)
\end{aligned}$$

For short notations, we denote the above Eq. (3.4) by $\sum_{m=1}^5 LHS^m=RHS$, and next let us estimate them term by term. First, it is easy to see that

$$LHS^1+LHS^4=\frac{1}{\Delta t}\|\overrightarrow{\psi}^{\,n}-\overrightarrow{\psi}^{\,n-1}\|_{U,2}^2+\frac{1}{\Delta t}\|\overrightarrow{A}^{\,n}-\overrightarrow{A}^{\,n-1}\|_{W,2}^2\,.$$

The the real part of the term LHS^2 can be rewritten by

$$\begin{aligned}
\mathrm{Re}\left[LHS^2\right]&=\frac12\sum_{jk}\frac{hh'_{jk}}{\kappa^2}\left\{\frac{|\psi_j^n-\psi_k^n\exp(-i\kappa a_{jk}^n h)|^2}{h^2}-\frac{|\psi_j^{n-1}-\psi_k^{n-1}\exp(-i\kappa a_{jk}^{n-1}h)|^2}{h^2}\right\}\\
&\quad-\frac12\sum_{jk}\frac{h'_{jk}}{h\kappa^2}\Big\{|\psi_k^n|^2+|\psi_j^n|^2-2\mathrm{Re}[\psi_k^n\exp(-i\kappa a_{jk}^n h)(\psi_j^n)^*]-|\psi_k^{n-1}|^2-|\psi_j^{n-1}|^2\\
&\quad+2\mathrm{Re}[\psi_k^{n-1}\exp(-i\kappa a_{jk}^{n-1}h)(\psi_j^{n-1})^*]+2\mathrm{Re}[\psi_k^n\exp(-i\kappa a_{jk}^n h)(\psi_j^n)^*]-2|\psi_j^n|^2\\
&\quad-2\mathrm{Re}[\psi_k^n\exp(-i\kappa a_{jk}^n h)(\psi_j^{n-1})^*]+2\mathrm{Re}[\psi_j^n(\psi_j^{n-1})^*]+2\mathrm{Re}[\psi_j^n\exp(i\kappa a_{jk}^n h)(\psi_k^n)^*]\\
&\quad-2|\psi_k^n|^2-2\mathrm{Re}[\psi_j^n\exp(i\kappa a_{jk}^n h)(\psi_k^{n-1})^*]+2\mathrm{Re}[\psi_k^n(\psi_k^{n-1})^*]\Big\}\\
&=\frac12\sum_{jk}\frac{hh'_{jk}}{\kappa^2}\left\{\frac{|\psi_j^n-\psi_k^n\exp(-i\kappa a_{jk}^n)|^2}{h^2}-\frac{|\psi_j^{n-1}-\psi_k^{n-1}\exp(-i\kappa a_{jk}^{n-1})|^2}{h^2}\right\}+I,
\end{aligned}$$

where

$$\begin{aligned}
I=\frac12\sum_{jk}\frac{h'_{jk}}{h\kappa^2}\Big\{&2\mathrm{Re}[\psi_k^{n-1}(\psi_j^{n-1})^*\big(\exp(-i\kappa a_{jk}^{n-1}h)-\exp(-i\kappa a_{jk}^n h)]\big)\\
&-|(\psi_k^n-\psi_k^{n-1})\exp(-i\kappa a_{jk}^n h)-(\psi_k^n-\psi_k^{n-1})^2|^2\Big\}\,.
\end{aligned}$$

By using the fact that $\mathrm{Re}[i\psi_j^n(\psi_j^n)^*]=\mathrm{Re}[i\psi_j^{n-1}(\psi_j^{n-1})^*]=0$, we then get

$$\begin{aligned}
I&\le\frac12\sum_{jk}\frac{h'_{jk}}{h\kappa^2}\Big\{2\mathrm{Re}[\psi_k^{n-1}(\psi_j^{n-1})^*\big(\exp(-i\kappa a_{jk}^{n-1}h)-\exp(-i\kappa a_{jk}^n h)]\big)\Big\}\\
&=\sum_{jk}\frac{h\,h'_{jk}}{\kappa^2}\mathrm{Re}\Big[\Big(\frac{\psi_k^{n-1}\exp(-i\kappa a_{jk}^{n-1}h)-\psi_j^{n-1}}{h^2}\Big)(\psi_j^{n-1})^*\big(1-\exp\big(-i\kappa(a_{jk}^n-a_{jk}^{n-1})h\big)\Big]
\end{aligned}$$

$$
\begin{aligned}
&+\sum_{jk}\frac{h\,h'_{jk}}{\kappa^2}\mathrm{Re}\Big[\psi_j^{n-1}(\psi_j^{n-1})^*\Big(\frac{1-\exp\big(-i\kappa(a_{jk}^n-a_{jk}^{n-1})h\big)-i\kappa(a_{jk}^n-a_{jk}^{n-1})h}{h^2}\Big)\Big]\\
\le&\sum_{jk}\frac{h\,h'_{jk}}{\kappa^2}\Big\{\frac{|\psi_k^{n-1}\exp(-i\kappa a_{jk}^{n-1}h)-\psi_j^{n-1}|}{h}\kappa|a_{jk}^n-a_{jk}^{n-1}|+\kappa^2|a_{jk}^n-a_{jk}^{n-1}|^2\Big\}\\
\le&\ \Delta t\sum_{jk}\frac{h\,h'_{jk}}{\kappa^2}\frac{|\psi_k^{n-1}\exp(-i\kappa a_{jk}^{n-1}h)-\psi_j^{n-1}|^2}{h^2}+\sum_{jk}h\,h'_{jk}(1+\frac{1}{4\Delta t})|a_{jk}^n-a_{jk}^{n-1}|^2\,.
\end{aligned}
\tag{3.5}
$$

Therefore, taking (3.5) into the estimate for LHS^2, we arrive at

$$
\begin{aligned}
\mathrm{Re}\big[LHS^2\big]\ge&\ \frac{1}{2}\sum_{jk}\frac{hh'_{jk}}{\kappa^2}\Big\{\frac{|\psi_j^n-\psi_k^n\exp(-i\kappa a_{jk}^n)|^2}{h^2}-\frac{|\psi_j^{n-1}-\psi_k^{n-1}\exp(-i\kappa a_{jk}^{n-1})|^2}{h^2}\Big\}\\
&-\Delta t\sum_{jk}\frac{h\,h'_{jk}}{\kappa^2}\Big\{\frac{|\psi_k^n\exp(-i\kappa a_{jk}^n h)-\psi_j^n|^2}{h^2}+\frac{|\psi_k^{n-1}\exp(-i\kappa a_{jk}^{n-1}h)-\psi_j^{n-1}|^2}{h^2}\Big\}\\
&-\sum_{jk}h\,h'_{jk}\left(1+\frac{1}{4\Delta t}\right)|a_{jk}^n-a_{jk}^{n-1}|^2\,.
\end{aligned}
$$

The real part of the cubic nonlinear term LHS^3 can be bounded by

$$
\begin{aligned}
\mathrm{Re}\Big[LHS^3\Big]=&\sum_j\frac{|\tau'_j|}{2}\ \Big((|\psi_j^{n-1}|^2-1)\big(|\psi_j^n|^2-|\psi_j^{n-1}|^2+|\psi_j^n-\psi_j^{n-1}|^2\big)+\alpha(|\psi_j^n-\psi_j^{n-1}|^2)\Big)\\
=&\sum_j\frac{|\tau'_j|}{2}\Big(|\psi_j^{n-1}|^2-1\Big)\Big(|\psi_j^n|^2-1\Big)-\sum_j\frac{|\tau'_j|}{2}\Big(|\psi_j^{n-1}|^2-1\Big)^2\\
&+\sum_j\frac{|\tau'_j|}{2}\Big(|\psi_j^{n-1}|^2-1\Big)|\psi_j^n-\psi_j^{n-1}|^2+\alpha\sum_j\frac{|\tau'_j|}{2}|\psi_j^n-\psi_j^{n-1}|^2\\
=&\sum_j\frac{|\tau'_j|}{4}\Big(|\psi_j^n|^2-1\Big)^2-\sum_j\frac{|\tau'_j|}{4}\Big(|\psi_j^{n-1}|^2-1\Big)^2\\
&+\sum_j\frac{|\tau'_j|}{4}\Big\{\Big(2|\psi_j^{n-1}|^2-2+2\alpha\Big)|\psi_j^n-\psi_j^{n-1}|^2-\Big(|\psi_j^{n-1}|+|\psi_j^n|\Big)^2(|\psi_j^{n-1}|-|\psi_j^n|)^2\Big\}\\
\ge&\sum_j\frac{|\tau'_j|}{4}\Big(|\psi_j^n|^2-1\Big)^2-\sum_j\frac{|\tau'_j|}{4}\Big(|\psi_j^{n-1}|^2-1\Big)^2+\Big(\frac{\alpha}{2}-\frac{3}{2}\Big)\sum_j|\tau'_j||\psi_j^n-\psi_j^{n-1}|^2
\end{aligned}
$$

where the fact of $|\psi_j^n|\le 1$ has been used. By Lemma 2.1, we have that

$$
\begin{aligned}
LHS^5&=\Big\langle\nabla_h^\perp(\overrightarrow{c}^{\,n}-\overrightarrow{H}),\ \overrightarrow{A}^{n}-\overrightarrow{A}^{n-1}\Big\rangle_W\\
&=\frac{1}{2}\Big(\|C_h\overrightarrow{A}^{n}-\overrightarrow{H}\|_{V,2}^2-\|C_h\overrightarrow{A}^{n-1}-\overrightarrow{H}\|_{V,2}^2+\|C_h(\overrightarrow{A}^{n}-\overrightarrow{A}^{n-1})\|_{V,2}^2\Big)\,.
\end{aligned}
$$

Next, we turn to the right hand side of (3.4). Note that

$$
\mathrm{Re}[i\,\psi_j^{n-1}(\psi_j^{n-1})^*]=0\quad\text{and}\quad|\psi_j^n|\le 1\,,
$$

thus RHS can be bounded by

$$\begin{aligned} RHS &= \sum_{jk} \frac{h\,h'_{jk}}{\kappa} \mathrm{Re}\Big[-i\,\frac{\psi_k^{n-1}\exp(-i\kappa a_{jk}^{n-1}h) - \psi_j^{n-1}}{h} (\psi_j^{n-1})^*(a_{jk}^n - a_{jk}^{n-1}) \Big] \\ &\le \sum_{jk} \frac{h\,h'_{jk}}{\kappa^2} \frac{|\psi_k^{n-1}\exp(-i\kappa a_{jk}^{n-1}h) - \psi_j^{n-1}|}{h} \kappa |a_{jk}^n - a_{jk}^{n-1}| \\ &\le \sum_{jk} h\,h'_{jk} \frac{|a_{jk}^n - a_{jk}^{n-1}|^2}{4\Delta t} + \Delta t \sum_{jk} h\,h'_{jk} \frac{|\psi_k^{n-1}\exp(-i\kappa a_{jk}^{n-1}h) - \psi_j^{n-1}|^2}{\kappa^2 h^2}\,. \end{aligned}$$

Finally, taking all the above estimates for $\{LHS^k\}_{k=1}^5$ and RHS into (3.4) gives

$$\begin{aligned} &\mathcal{G}^h(\overrightarrow{\psi}^n, \overrightarrow{A}^n) - \mathcal{G}^h(\overrightarrow{\psi}^{n-1}, \overrightarrow{A}^{n-1}) + \frac{1}{\Delta t} \left\{ \| \overrightarrow{\psi}^n - \overrightarrow{\psi}^{n-1} \|_{U,2}^2 + \| \overrightarrow{A}^n - \overrightarrow{A}^{n-1} \|_{W,2}^2 \right\} \\ &\le 4\Delta t \left(\mathcal{G}^h(\overrightarrow{\psi}^n, \overrightarrow{A}^n) + \mathcal{G}^h(\overrightarrow{\psi}^{n-1}, \overrightarrow{A}^{n-1}) \right) + \left(1 + \frac{1}{4\Delta t} \right) \| \overrightarrow{A}^n - \overrightarrow{A}^{n-1} \|_{U,2}^2 \\ &\quad + \left(\frac{3}{2} - \frac{\alpha}{2} + \frac{1}{4\Delta t} \right) \| \overrightarrow{\psi}^n - \overrightarrow{\psi}^{n-1} \|_{U,2}^2\,. \end{aligned}$$

Thanks to the discrete Gronwall's inequality, for any fixed $\alpha > 0$, we can conclude that for $\Delta t < 1/4$

$$\mathcal{G}^h(\overrightarrow{\psi}^n, \overrightarrow{A}^n) + \sum_{m=1}^n \frac{1}{\Delta t} \left\{ \left\| \overrightarrow{\psi}^m - \overrightarrow{\psi}^{m-1} \right\|_{U,2}^2 + \left\| \overrightarrow{A}^m - \overrightarrow{A}^{m-1} \right\|_{W,2}^2 \right\} \le C\mathcal{G}^h(\overrightarrow{\psi}^0, \overrightarrow{A}^0)\,, \tag{3.6}$$

which directly gives the energy estimate (3.3). □

Remark 3.3 It should be noted that the above energy stability (3.6) does not rely on the stabilizing parameter α. A similar energy stability result like that stated in Theorem 3.2 also can be proven for the stabilized semi-implicit Lorentz gauge scheme (2.33)–(2.34).

4 Relations to the Lowest Order Rectangular Nédélec Edge Element Approximation

4.1 The Zero-Electric Potential Gauge Scheme

A key observation is that the discretization (2.25) for $\mathbf{A}$ in the zero-electric potential gauge scheme can be interpreted within the framework of the finite element method using the Nédélec edge element [30]. The four basis functions of the lowest order rectangular Nédélec edge element defined on the reference element $[0, 1]^2$ are shown in Fig. 2.

Let $S_h \in H^1$ be the lowest order bilinear finite element space and let $V_h \in \mathbf{H}(\mathrm{curl}(\Omega))$ be the finite element space with the lowest order Nédélec edge element on Γ_h. We can easily verify that the degrees of freedom of V_h equals to N_1, which is the same to the unknowns $\{a_{jk}\}$, and S_h has the N_0 unknowns which equals to that of $\{\Phi_j\}$(or $\{d_j\}$). If the unknowns $\{a_{jk}\}$ for (2.25) and $\mathbf{A}_h \in V_h$ are ordered in the same fashion globally, then there exists a one to one map $\mathbf{A}_h \to \overrightarrow{A}$ for each $\mathbf{A}_h \in V_h$. Moreover, for given $(\overrightarrow{\psi}^{n-1}, \overrightarrow{A}^{n-1})$, we can define a unique function $\mathbf{F}_h \in V_h$ such that

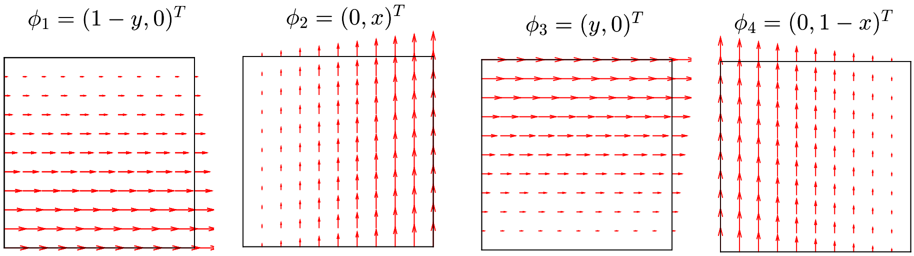

Fig. 2 An illustration of the four basis functions of the lowest order rectangular Nédélec edge element of first family

$$\mathbf{F}_h = \frac{1}{h\,\kappa}\mathrm{Re}\left[i(\psi_k^{n-1})^*\psi_j^{n-1}\exp(i\kappa a_{jk}^{n-1}h)\right] \quad \text{at the center of edge } \{s_{jk}\}.$$

A semi-implicit finite element method for (2.20) is to look for $\mathbf{A}_h^n \in V_h$ such that

$$\left(\frac{\mathbf{A}_h^n - \mathbf{A}_h^{n-1}}{\Delta t}, \boldsymbol{v}_h\right) + (\mathrm{curl}\,\mathbf{A}_h^n - H, \mathrm{curl}\,\boldsymbol{v}_h) = (\mathbf{F}_h, \boldsymbol{v}_h)\ , \quad \forall \boldsymbol{v}_h \in V_h, \tag{4.1}$$

where we have used the boundary condition $\mathrm{curl}\mathbf{A}_h = H$ on $\partial\Omega$. To build a connection between the above FEM (4.1) and (2.25), we shall introduce a mass-lumped version FEM for $\mathbf{A}$. To simply the presentation, we define the quadrature formula

$$Q_{\tau,h}(f) = \frac{1}{4}\mathrm{area}(\tau)\Big[f(\boldsymbol{x}_j) + f(\boldsymbol{x}_k) + f(\boldsymbol{x}_l) + f(\boldsymbol{x}_m)\Big] \approx \int_\tau f\,\mathrm{d}x.$$

Moreover, we define approximations of the inner products in S_h and V_h by

$$(u,v)_h = \sum_{\tau\in\Gamma_h} Q_{\tau,h}(u\cdot v), \quad \forall\, \boldsymbol{u},\boldsymbol{v} \in S_h; \qquad (\boldsymbol{w},\boldsymbol{v})_h = \sum_{\tau\in\Gamma_h} Q_{\tau,h}(\boldsymbol{w}\cdot\boldsymbol{v}), \quad \forall\, \boldsymbol{w},\boldsymbol{v} \in V_h, \tag{4.2}$$

where one can easily verify that (4.2) give a diagonal mass matrix for both finite element spaces S_h and V_h. For an element τ_{jklm} with nodes $\{\boldsymbol{x}_j, \boldsymbol{x}_k, \boldsymbol{x}_l, \boldsymbol{x}_m\}$ and edge length h, its element stiffness and mass matrices are defined respectively by

$$\mathbf{K}_2\big|_{\tau_{jklm}} = \begin{bmatrix} 1 & 1 & -1 & -1 \\ 1 & 1 & -1 & -1 \\ -1 & -1 & 1 & 1 \\ -1 & -1 & 1 & 1 \end{bmatrix} \tag{4.3}$$

$$\mathbf{M}\big|_{\tau_{jklm}} = \begin{bmatrix} \frac{h^2}{3} & 0 & \frac{h^2}{6} & 0 \\ 0 & \frac{h^2}{3} & 0 & \frac{h^2}{6} \\ \frac{h^2}{6} & 0 & \frac{h^2}{3} & 0 \\ 0 & \frac{h^2}{6} & 0 & \frac{h^2}{3} \end{bmatrix} \xrightarrow{\text{mass lumping}} \widetilde{\mathbf{M}}\big|_{\tau_{jklm}} = \frac{h^2}{2}\mathbf{I}_4, \tag{4.4}$$

Based on the above quadrature rule, we can rewrite (4.1) into a mass-lumped FEM as follows

$$\left(\frac{\mathbf{A}_h^n - \mathbf{A}_h^{n-1}}{\Delta t}, \boldsymbol{v}_h\right)_h + (\mathrm{curl}\,\mathbf{A}_h^n - H, \mathrm{curl}\,\boldsymbol{v}_h) = (\mathbf{F}_h, \boldsymbol{v}_h)_h\ , \quad \forall \boldsymbol{v}_h \in V_h. \tag{4.5}$$

The matrix form of the above mass-lumped FEM is

$$\frac{1}{\Delta t}\overrightarrow{A}^n + \widetilde{\mathbf{M}}^{-1}\mathbf{K}_2\overrightarrow{A}^n = \frac{1}{\Delta t}\overrightarrow{A}^{n-1} + \widetilde{\mathbf{M}}^{-1}\mathbf{E}_2\overrightarrow{H} + \widetilde{\mathbf{M}}^{-1}\overrightarrow{F}, \tag{4.6}$$

where $\overrightarrow{F}$ denotes the nonlinear term. In (4.6), $\mathbf{K}_2$ is the stiffness matrix and $\widetilde{\mathbf{M}}$ is the lumped mass matrix, respectively, which are generated by assembling the element mass and stiffness matrices in (4.3) and (4.4). We finally have the following equivalence

$$\widetilde{\mathbf{M}}^{-1}\mathbf{K}_2 = \mathbf{K}_1, \quad \widetilde{\mathbf{M}}^{-1}\mathbf{E}_2 = \mathbf{E}_1, \quad \widetilde{\mathbf{M}}^{-1}\overrightarrow{F} = \overrightarrow{N}(\overrightarrow{\psi}^{n-1}, \overrightarrow{A}^{n-1}), \tag{4.7}$$

where the matrices $\mathbf{K}_1, \mathbf{E}_1$ and the vectors $\overrightarrow{N}(\overrightarrow{\psi}^{n-1}, \overrightarrow{A}^{n-1})$ are define in (2.26). Therefore, the proposed semi-implicit gauge-invariant finite difference scheme (2.25) in space can be viewed as the mass-lumped lowest order Nédélec edge finite element methods by lumping all masses in one row into the diagonal entry (or using a special numerical quadrature). We refer to [36, Chapter 15] for more discussion on mass-lumped FEMs. We also remark that Christiansen and Halvorsen [8] proposed a gauge invariant finite element method for the Schrödinger eigenvalue problem in an electromagnetic field by using the mass-lumping technique, where certain requirement is needed for the mesh. It also should be noted that the covariant gradient of ψ used in [8] is defined as $\mathrm{grad}_A\psi = \nabla\psi + iA\psi$, which is similar to the term $\frac{i}{\kappa}\nabla\psi + \mathbf{A}\psi$ in the TDGL equations. Therefore, the numerical methods developed in [8] might be applied to the TDGL Eqs. (1.1)–(1.2).

4.2 The Lorentz Gauge Scheme

The main difference between the zero-electric potential gauge and the Lorentz gauge is that a term $-\nabla\mathrm{div}\mathbf{A}$ appears in (2.29) for $\mathbf{A}$ under the Lorentz gauge, which implies that $\mathbf{A} \in \mathbf{H}(\mathrm{div}) \cap \mathbf{H}(\mathrm{curl})$ in space. However, at first glance, the term $-(\nabla_h D_h \overrightarrow{A}^n)_{jk}$ in (2.34) denoting the discretization of $-\nabla\mathrm{div}\mathbf{A}$ is not compatible in the framework of Nédélec edge element, which is only $\mathbf{H}(\mathrm{curl})$ conforming. To this end, we turn to mixed FEMs to show the equivalence. In [26], a class of mixed FEMs is investigated for the Lorentz gauge TDGL equations, where the basic idea is to introduce $\Phi = -\mathrm{div}\,\mathbf{A}$ as an extra variable. Then, Lagrange elements and Nédélec edge elements are used to approximate Φ and $\mathbf{A}$, respectively. To incorporate with the current rectangular mesh, we consider a mixed method based on the lowest order bilinear element and lowest order rectangular Nédélec edge element.

By introducing $\Phi = -\mathrm{div}\,\mathbf{A}$ as an extra variable, a semi-implicit mixed FEM for (2.29) is to look for $(\Phi_h^n, \mathbf{A}_h^n) \in S_h \times V_h$ such that

$$(\Phi_h^n\,,\, w_h) - (\mathbf{A}_h^n, \nabla w_h) = 0, \quad \forall w_h \in S_h, \tag{4.8}$$

$$\left(\frac{\mathbf{A}_h^n - \mathbf{A}_h^{n-1}}{\Delta t}, \boldsymbol{v}_h\right) + (\nabla\Phi^n\,,\, \boldsymbol{v}_h) + (\mathrm{curl}\,\mathbf{A}_h^n - H, \mathrm{curl}\,\boldsymbol{v}_h) = (\mathbf{F}_h, \boldsymbol{v}_h)\ , \quad \forall \boldsymbol{v}_h \in V_h, \tag{4.9}$$

where we have used the boundary condition $\mathrm{curl}\mathbf{A}_h = H$ and $\mathbf{A}\cdot\mathbf{n} = 0$ on $\partial\Omega$. A mass-lumped version of the above FEM is to look for $(\Phi_h^n, \mathbf{A}_h^n) \in S_h \times V_h$ such that

$$(\Phi_h^n\,,\, w_h)_h - (\mathbf{A}_h^n, \nabla w_h)_h = 0, \quad \forall w_h \in S_h, \tag{4.10}$$

$$\left(\frac{\mathbf{A}_h^n - \mathbf{A}_h^{n-1}}{\Delta t}, \boldsymbol{v}_h\right)_h + (\nabla\Phi_h^n\,,\, \boldsymbol{v}_h)_h + (\mathrm{curl}\,\mathbf{A}_h^n - H, \mathrm{curl}\,\boldsymbol{v}_h) = (\mathbf{F}_h, \boldsymbol{v}_h)_h\ , \quad \forall \boldsymbol{v}_h \in V_h. \tag{4.11}$$

It should be pointed out that, due to the fact $\nabla S_h \subset V_h$ [2], the two terms $(\mathbf{A}_h^n, \nabla w_h)_h$ and $(\nabla\Phi^n\,,\, \boldsymbol{v}_h)_h$ are well-defined. We shall give a more compact matrix form for (4.11)–(4.11) later. Before going further, we present the local mass matrix for the lowest order bilinear element space S_h. Given an element τ_{jklm} with and edge length h, its element mass matrix and the corresponding mass-lumping version are defined by

$$\mathbf{M}_{\text{bilinear}}\Big|_{\tau_{jklm}} = h^2 \begin{bmatrix} \frac{1}{9} & \frac{1}{18} & \frac{1}{36} & \frac{1}{18} \\ \frac{1}{18} & \frac{1}{9} & \frac{1}{18} & \frac{1}{36} \\ \frac{1}{36} & \frac{1}{18} & \frac{1}{9} & \frac{1}{18} \\ \frac{1}{18} & \frac{1}{36} & \frac{1}{18} & \frac{1}{9} \end{bmatrix} \xrightarrow{\text{mass lumping}} \widetilde{\mathbf{M}}_{\text{bilinear}}\Big|_{\tau_{jklm}} = \frac{h^2}{4}\mathbf{I}_4 . \tag{4.12}$$

Then, we can rewrite (4.10) into a matrix form

$$\widetilde{\mathbf{M}}_{\text{bilinear}} \overrightarrow{\Phi}^n = \widetilde{\mathbf{D}} \overrightarrow{A}^n, \quad \text{i.e.,} \quad \overrightarrow{\Phi}^n = \widetilde{\mathbf{M}}_{\text{bilinear}}^{-1} \widetilde{\mathbf{D}} \overrightarrow{A}^n,$$

which immediately yields the following matrix form for $\mathbf{A}_h^n$

$$\frac{1}{\Delta t}\overrightarrow{A}^n + \widetilde{\mathbf{M}}^{-1}\widetilde{\mathbf{D}}^T\widetilde{\mathbf{M}}_{\text{bilinear}}^{-1}\widetilde{\mathbf{D}}\overrightarrow{A}^n + \widetilde{\mathbf{M}}^{-1}\mathbf{K}_2\overrightarrow{A}^n = \frac{1}{\Delta t}\overrightarrow{A}^{n-1} + \widetilde{\mathbf{M}}^{-1}\mathbf{E}_2\overrightarrow{H} + \widetilde{\mathbf{M}}^{-1}\overrightarrow{F}, \tag{4.13}$$

where $\widetilde{\mathbf{M}}$, $\mathbf{K}_2$, $\mathbf{E}_2$, $\overrightarrow{H}$ and $\overrightarrow{F}$ are the same to those in the zero-electric potential gauge case. Recall the definition of ∇_h in (2.1) and D_h in (2.5), we claim that

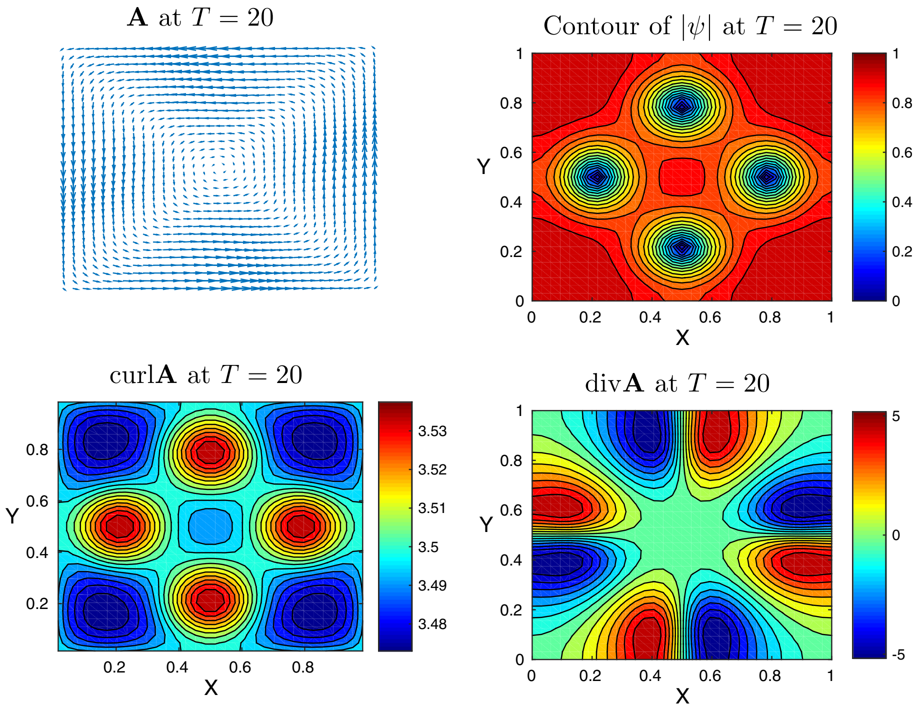

Fig. 3 Simulation results at $T = 20$ by the stabilized semi-implicit zero-electric potential gauge scheme (2.24)–(2.25) with $\Delta t = 0.1$ and $h = \frac{1}{64}$ for Example 5.1

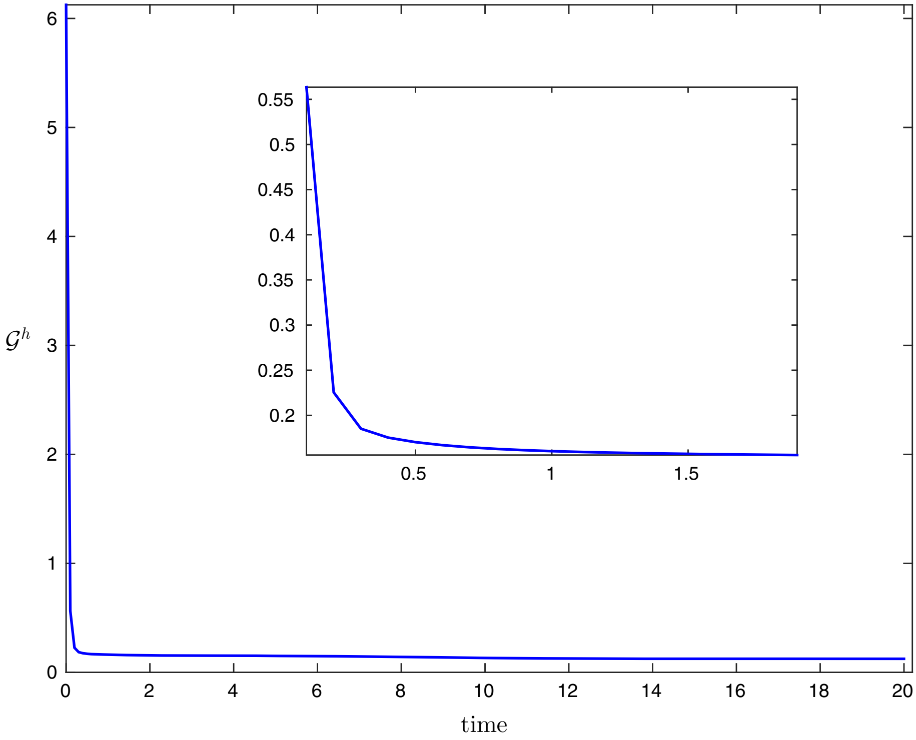

Fig. 4 Energy evolution obtained by the stabilized semi-implicit zero-electric potential gauge scheme (2.24)–(2.25) with $\Delta t = 0.1$ and $h = \frac{1}{64}$ for Example 5.1

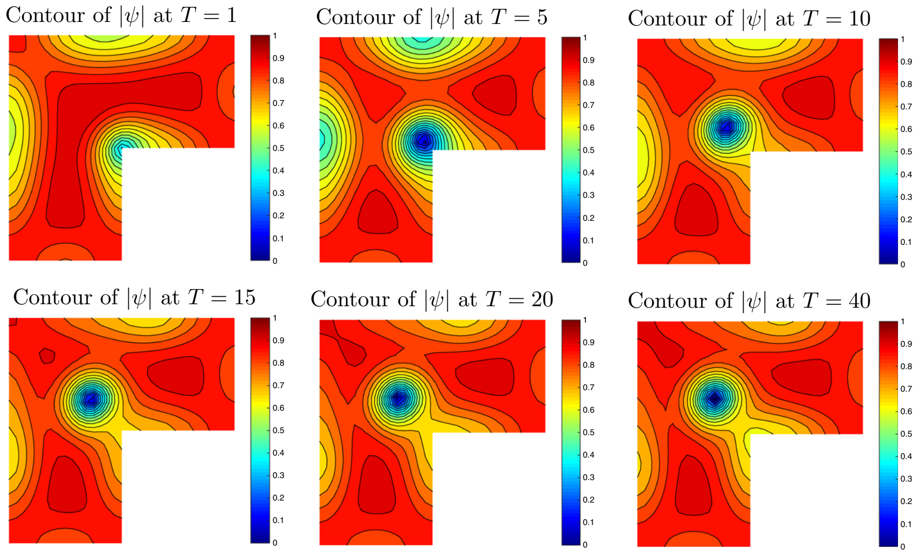
Contour of $|\psi|$ at $T = 1$

Contour of $|\psi|$ at $T = 5$

Contour of $|\psi|$ at $T = 10$

Contour of $|\psi|$ at $T = 15$

Contour of $|\psi|$ at $T = 20$

Contour of $|\psi|$ at $T = 40$

Fig. 5 Plots of the contour of simulated $|\psi|$ at time $T = 1, 5, 15, 20, 20$ and 40 by the stabilized semi-implicit zero-electric potential gauge scheme (2.24)–(2.25) with $\Delta t = 0.1$ and $h = \frac{1}{64}$ for Example 5.2 with $H = 5$

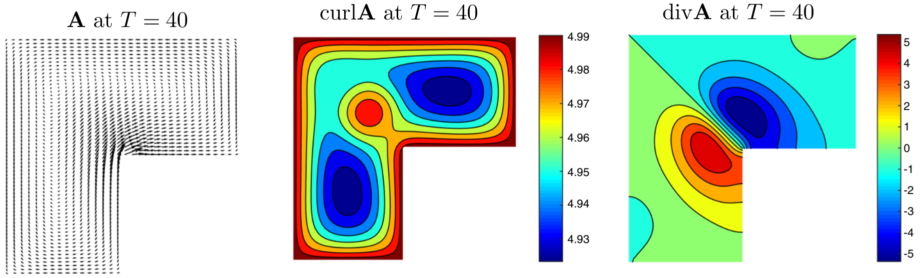
$\mathbf{A}$ at $T = 40$ curl$\mathbf{A}$ at $T = 40$ div$\mathbf{A}$ at $T = 40$

Fig. 6 Plots of simulated $\mathbf{A}$, curl$\mathbf{A}$ and div$\mathbf{A}$ at time $T = 40$ by the stabilized semi-implicit zero-electric potential gauge scheme (2.24)–(2.25) with $\Delta t = 0.1$ and $h = \frac{1}{64}$ for Example 5.2 with $H = 5$

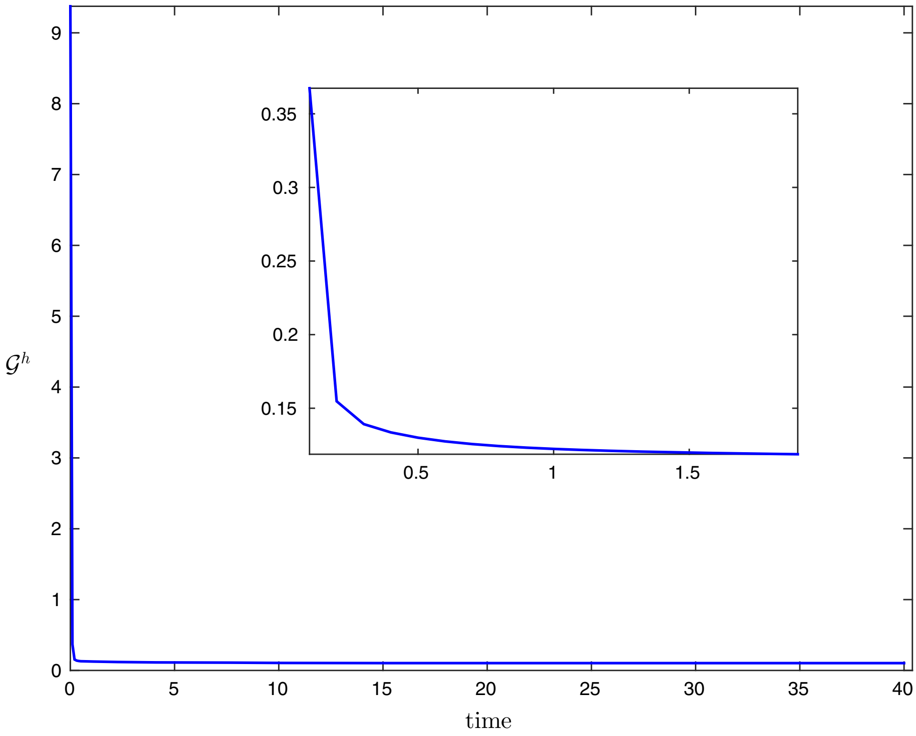

Fig. 7 Energy evolution obtained by the stabilized semi-implicit zero-electric potential gauge scheme (2.24)–(2.25) with $\Delta t = 0.1$ and $h = \frac{1}{64}$ for Example 5.2 with $H = 5$

$$\nabla_h = \widetilde{\mathbf{M}}^{-1}\widetilde{\mathbf{D}}^T, \quad -D_h = \widetilde{\mathbf{M}}_{\text{bilinear}}^{-1}\widetilde{\mathbf{D}},$$

and therefore $-\nabla_h D_h = \widetilde{\mathbf{M}}^{-1}\widetilde{\mathbf{D}}^T\widetilde{\mathbf{M}}_{\text{bilinear}}^{-1}\widetilde{\mathbf{D}}$. Thus, we observe that the Lorentz gauge scheme (2.34) is a mass-lumped mixed FEM.

In "Appendix A", we provide a concrete example with explicit matrices and entries on a uniform 2×2 mesh to demonstrate the equivalence of the gauge invariant finite difference approximation and the mass-lumped mixed finite element method.

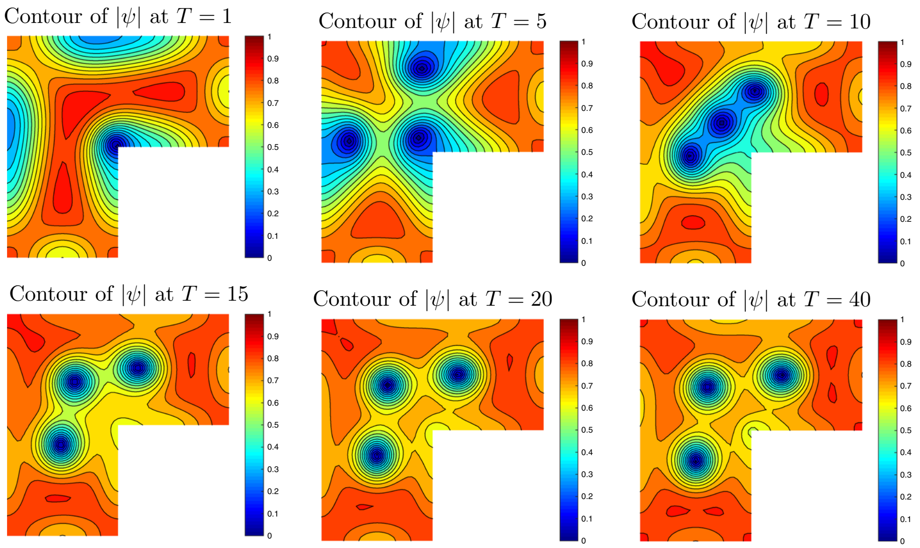

Fig. 8 Plots of the contour of simulated $|\psi|$ at time $T = 1, 5, 15, 20, 20$ and 40 by (2.24)–(2.25) with $\Delta t = 0.1$ and $h = \frac{1}{64}$ for Example 5.2 with $H = 7.2$

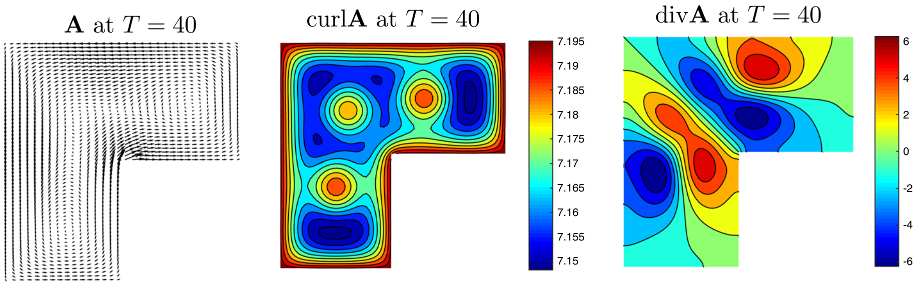

Fig. 9 Plots of simulated $\mathbf{A}$, curl$\mathbf{A}$ and div$\mathbf{A}$ at time $T = 40$ by the stabilized semi-implicit zero-electric potential gauge scheme (2.24)–(2.25) with $\Delta t = 0.1$ and $h = \frac{1}{64}$ for Example 5.2 with $H = 7.2$

5 Numerical Experiments

In this section, we provide some numerical experiments on vortex motion simulations for convex, non-convex and multi-connected domains to test the performance of the stabilized semi-implicit zero-electric potential gauge scheme (2.24)–(2.25) and the stabilized semi-implicit Lorentz gauge scheme (2.33)–(2.34). We set the stabilized parameter $\alpha = 2$ in all tests.

5.1 Tests of the Zero-Electric Potential Gauge Scheme

We first test the the stabilized semi-implicit zero-electric potential gauge scheme (2.24)–(2.25) for solving the TDGL equations.

Example 5.1 In the first example, we solve the TDGL equations to simulate the vortex motion in a unit square superconductor. Here we set $\Omega = (0, 1)^2$, the Ginzburg–Landau parameter

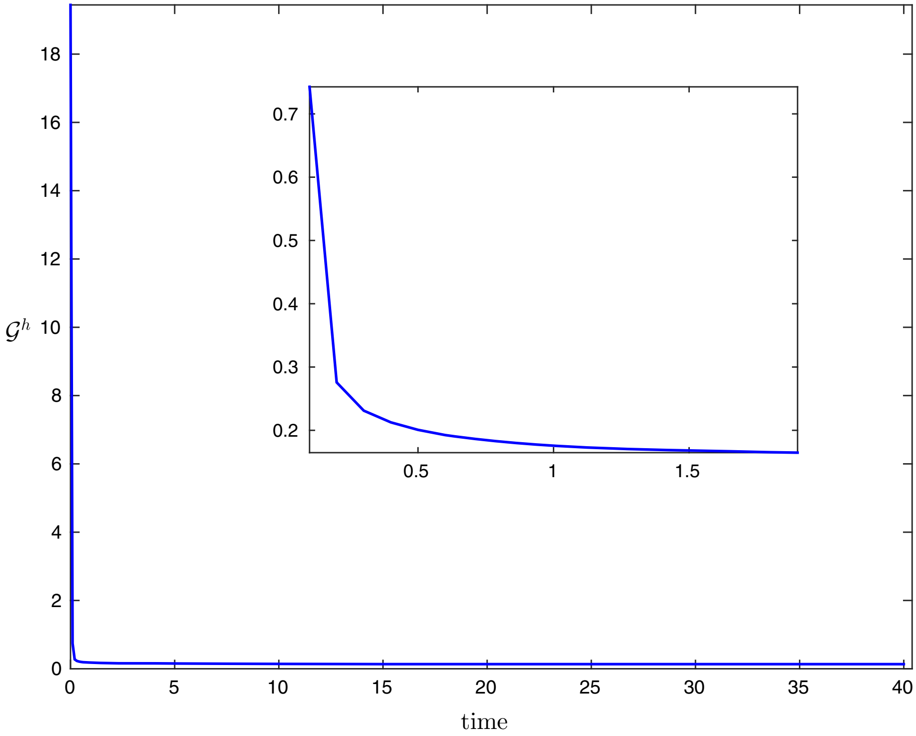

Fig. 10 Energy evolution obtained by the stabilized semi-implicit zero-electric potential gauge scheme (2.24)–(2.25) with $\Delta t = 0.1$ and $h = \frac{1}{64}$ for Example 5.2 with $H = 7.2$

$\kappa = 10$ and the external applied magnetic field $H = 3.5$. In the simulations, we set the time step size $\Delta t = 0.1$ and the spatial mesh size $h = \frac{1}{64}$. This benchmark problem has been used to test many other methods, e.g., conventional Lagrange finite element methods [10,16,31,32], mixed finite element methods [17], a method based on Hodge decomposition [27], and a method based on mixed formulation [18].

The simulation results of ψ and $\mathbf{A}$ at $T = 20$ computed by the zero-electric potential gauge scheme (2.24)–(2.25) are presented in Fig. 3 (top row). We observe that there are four vortices in the domain and the vortex pattern are stable near $T = 20$, which agree very well with the previous results reported in [10,16–18,27,31,32]. Moreover, Fig. 3 (bottom row) shows that the proposed stabilized semi-implicit gauge-invariant scheme is also able to compute the magnetic field curl$\mathbf{A}$ and the electric potential div$\mathbf{A}$ accurately. Furthermore, we plot the energy evolution in Fig. 4, which clearly shows that the discrete Ginzburg–Landau energy $\mathcal{G}^h(\overrightarrow{\psi}, \overrightarrow{A})$ is decreasing as time evolves.

Example 5.2 In the second example, we use the proposed scheme (2.24)–(2.25) to study the TDGL equations in an L-shape domain, where $\Omega = (-0.5, 0) \times (-0.5, 0.5) \cup (0, 0.5) \times (0, 0.5)$. We set $\kappa = 10$ and $H = 5$ and 7.2 respectively. This problem was also tested previously in [17,18,27], in which the main challenge is the low regularity of $\mathbf{A}$ due to the re-entrant corner; in particular, conventional finite element methods may converge to a "spurious" vortex pattern. In the simulations, we used the time step size $\Delta t = 0.1$ and the mesh size $h = \frac{1}{64}$.

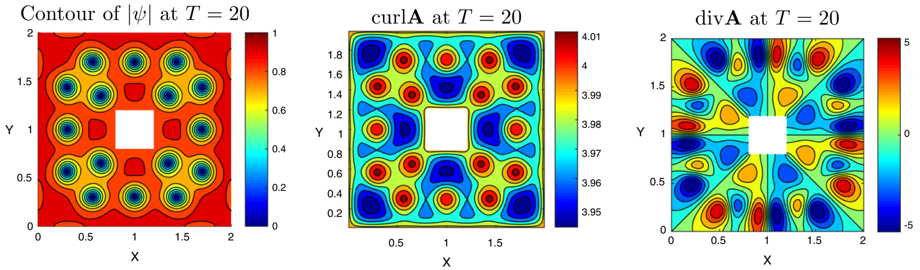
Contour of $|\psi|$ at $T = 20$

curl**A** at $T = 20$

div**A** at $T = 20$

Fig. 11 Plots of the contour of simulated $|\psi|$, curl**A** and div**A** at time $T = 20$ by the stabilized semi-implicit zero-electric potential gauge scheme (2.24)–(2.25) with $\Delta t = 0.05$ and $h = \frac{1}{80}$ for Example 5.3

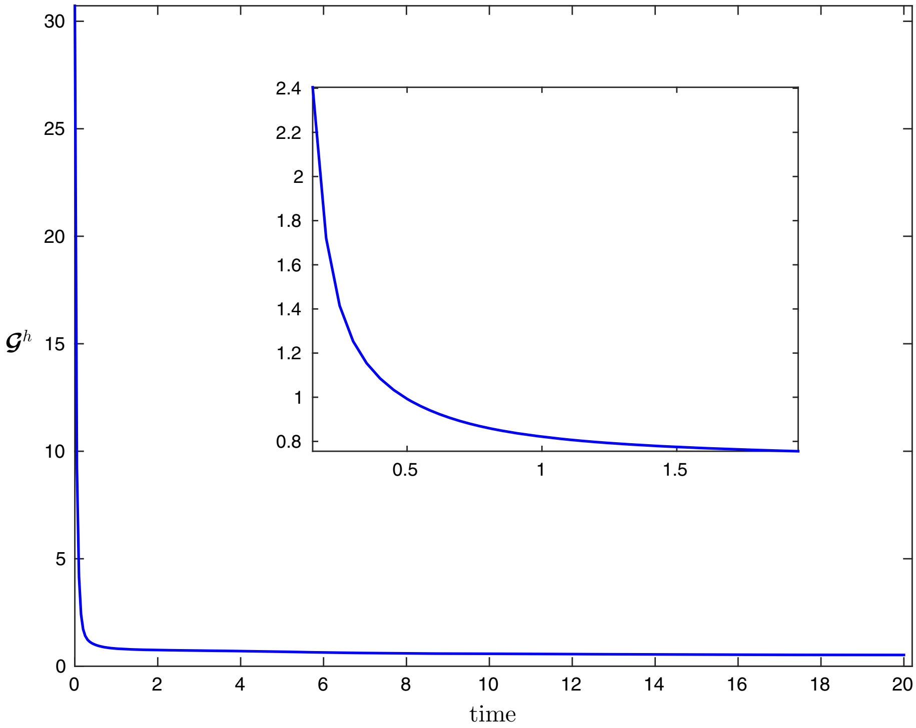

Fig. 12 Energy evolution obtained by the stabilized semi-implicit zero-electric potential gauge scheme (2.24)–(2.25) with $\Delta t = 0.05$ and $h = \frac{1}{80}$ for Example 5.3

The external applied magnetic field was first set to $H = 5$. The contour plots of simulated $|\psi|$ at time $T = 1, 5, 15, 20, 20$ and 40 are presented in Fig. 5, which agree well with the results reported in [17,18,27]. There is only one vertex in the stationary state for ψ. We also present plots of simulated **A** in Fig. 6, which clearly shows that **A** is singular near the origin $(0, 0)$. The magnetic field curl**A** and div **A** also agree well with the results obtained in [17]. Moreover, we plot the energy evolution in Fig. 7, which demonstrates that $\mathcal{G}^h(\overrightarrow{\psi}, \overrightarrow{A})$ is decreasing as time evolves for this non-convex domain.

It is well-known that a larger applied magnetic field H (under a certain critical value) can give more vortices. We show in Fig. 8 the results of simulated $|\psi|$ at time $T = 1, 5, 15, 20, 20$

and 40 under the same physical settings except the external applied magnetic field $H = 7.2$ now. It is observed that there are three vortices at the stationary state. The plots of $\mathbf{A}$, curl $\mathbf{A}$ and div $\mathbf{A}$ are shown in Fig. 9. The energy evolution plot is shown in in Fig. 10, which again confirms that the proposed scheme is energy stable.

Example 5.3 In the third example, we study the TDGL equations in a multi-connected domain. Here we set $\Omega = (0, 2)^2/[0.8, 1.2]^2$, the Ginzburg–Landau parameter $\kappa = 10$ and the external applied magnetic filed $H = 4$. In the simulations, we set the time step size $\Delta t = 0.05$ and the mesh size $h = \frac{1}{80}$.

Plots of the contour of simulated $|\psi|$, curl$\mathbf{A}$ and div $\mathbf{A}$ at $T = 20$ are shown in Fig. 11, which agree well with the results obtained by the mixed finite element method in [17]. The plots of numerical results obtained by the mixed finite element method [17] are omitted here. We also plot the energy evolution in Fig. 12, which shows the energy stability of the stabilized semi-implicit zero-electric potential gauge scheme (2.24)–(2.25).

5.2 Tests of the Lorentz Gauge Scheme

Now, we turn to the stabilized semi-implicit Lorentz gauge scheme (2.33)–(2.34). We first test its performance for Example 5.1. Note that the square domain is convex in this example and the exact solution satisfies the regularity assumption in [11]. The numerical results at $T = 20$ computed by the stabilized semi-implicit Lorentz potential gauge scheme (2.33)–(2.34) are presented in Fig. 13. It is easy to see that the vortex pattern agrees very well with

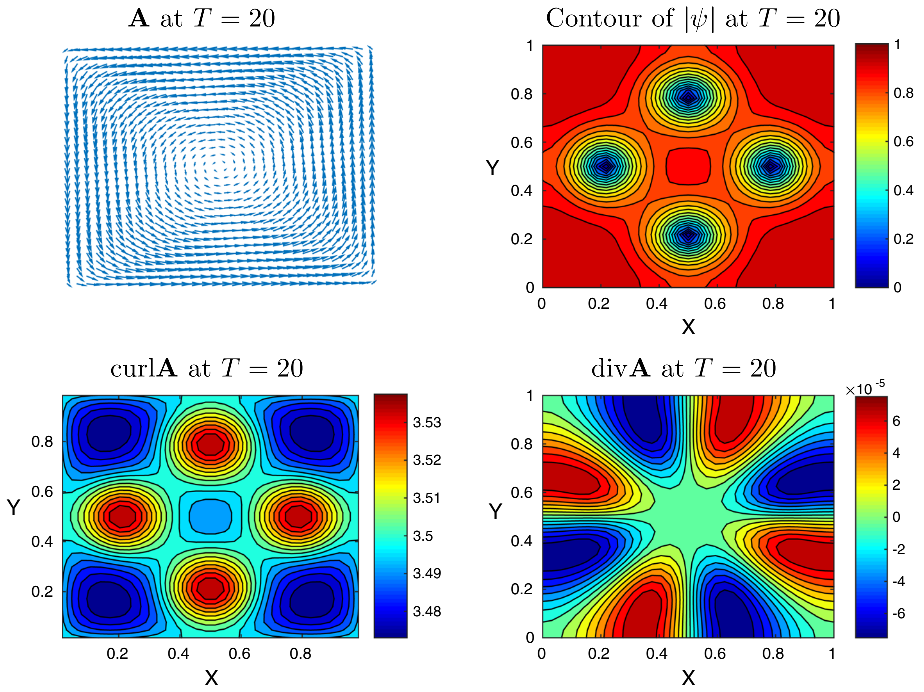

Fig. 13 Simulation results at $T = 20$ computed by stabilized semi-implicit Lorentz gauge scheme (2.33)–(2.34) with $\Delta t = 0.1$ and $h = \frac{1}{64}$ for Example 5.1

that in Fig. 3. Moreover, we observe that the amplitude of div **A** is relatively small in this case, which is around $O(10^{-5})$. The energy evolution plot obtained by the Lorentz gauge scheme (2.33)–(2.34) are shown in Fig. 14. We can see that it is the same to that in Fig. 4 computed by the zero-electric potential gauge scheme (2.24)–(2.25), which also confirms that the discrete Ginzburg–Landau energy $\mathcal{G}^h(\overrightarrow{\psi}, \overrightarrow{A})$ defined in (2.10) is gauge-invariant at the discrete level.

We next test Example 5.2. Note that the L-shape domain is non-convex in this example. We first set $H = 5$ and the contour plots of simulated $|\psi|$ at time $T = 1, 5, 15, 20, 20$ and 40 are shown in in Fig. 15, together the plots of simulated **A**, curl**A** and div **A** in Fig. 16. It should be noted that, the vortex pattern plots for $H = 5$ agree well with the results presented in Fig. 5 and in [17,18,27]. Moreover, the energy evolution figure is also the same to that of the zero-electric potential gauge scheme, see Fig. 17.

Then, we increase the external applied magnetic field to $H = 7.2$ and present in Fig. 18 the vortex pattern at time $T = 1, 5, 15, 20, 20$ and 40. We observe from Fig. 18 that there are three vortices, which is the same to the result of vortices in Fig. 8 obtained by the zero-electric potential gauge scheme. Moreover, the plots of simulated curl**A** and div **A** shown in Fig. 19 also agree with that in Fig. 9 obtained by the zero-electric potential gauge scheme. Thus, this example indicates that the Lorentz gauge scheme (2.33)–(2.34) is also able to give correct solutions for the TDGL equations in non-convex domains. We show the energy evolution in Fig. 20 and observe that it is the same to that in Fig. 10 obtained by the zero-electric potential gauge scheme.

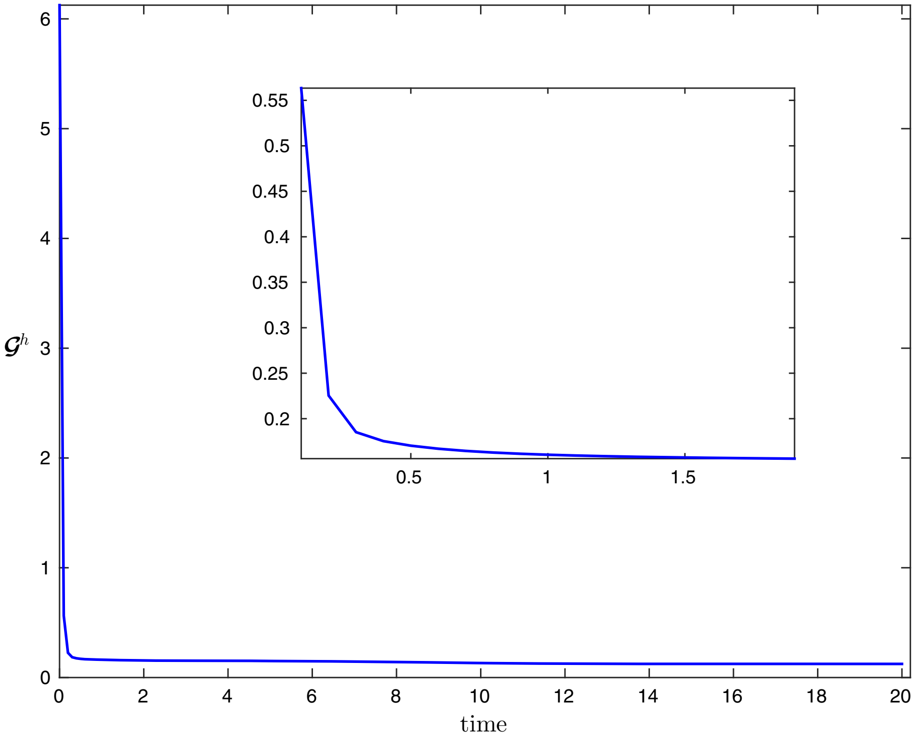

Fig. 14 Energy evolution obtained by the stabilized semi-implicit Lorentz gauge scheme (2.33)–(2.34) with $\Delta t = 0.1$ and $h = \frac{1}{64}$ for Example 5.1

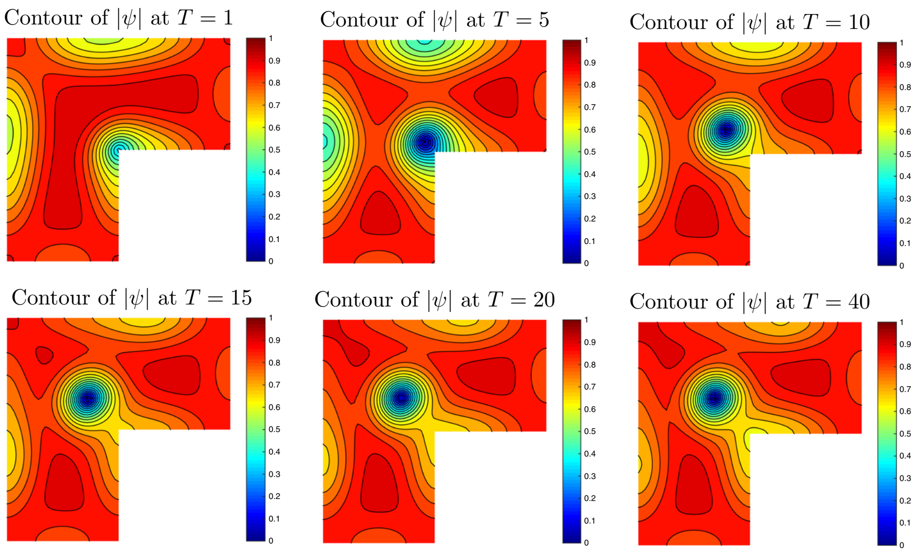

Fig. 15 Plots of the contour of simulated $|\psi|$ at time $T = 1, 5, 15, 20, 20$ and 40 by stabilized semi-implicit Lorentz gauge scheme (2.33)–(2.34) with $\Delta t = 0.1$ and $h = \frac{1}{64}$ for Example 5.2 with $H = 5$

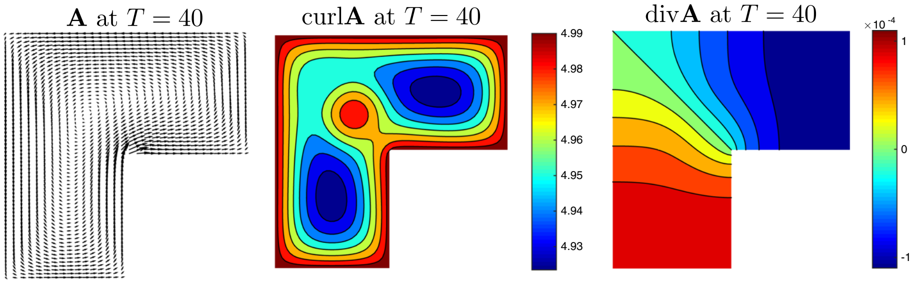

Fig. 16 Plots of simulated **A**, curl**A** and div**A** at time $T = 40$ by the stabilized semi-implicit Lorentz gauge scheme (2.33)–(2.34) with $\Delta t = 0.1$ and $h = \frac{1}{64}$ for Example 5.2 with $H = 5$

Finally, we test the performance of the Lorentz gauge scheme (2.33)–(2.34) for Example 5.3, where a multi-connected domain is used. It is easy to see that the inner square introduces four re-entrant corners, where the exact solution might be singular. Plots of the contour of simulated $|\psi|$, curl**A** and div**A** at $T = 20$ are shown in Fig. 21, which shows the same vortex pattern and vortex number in Fig. 11. The energy evolution is plot in Fig. 22, which is the same to that in Fig. 12. Thus, we demonstrate that the discrete Ginzburg–Landau energy (2.10) is gauge invariant for multi-connected domains. Numerical results indicate that the Lorentz gauge scheme (2.33)–(2.34) also works well for multi-connected domains.

6 Conclusions

In this paper we propose a stabilized semi-implicit Euler gauge-invariant method for solving the TDGL equations in the two-dimensional space. The proposed scheme is linear and preserves the point-wise bound $|\psi_h| \leq 1$ unconditionally and the energy stability. For the first

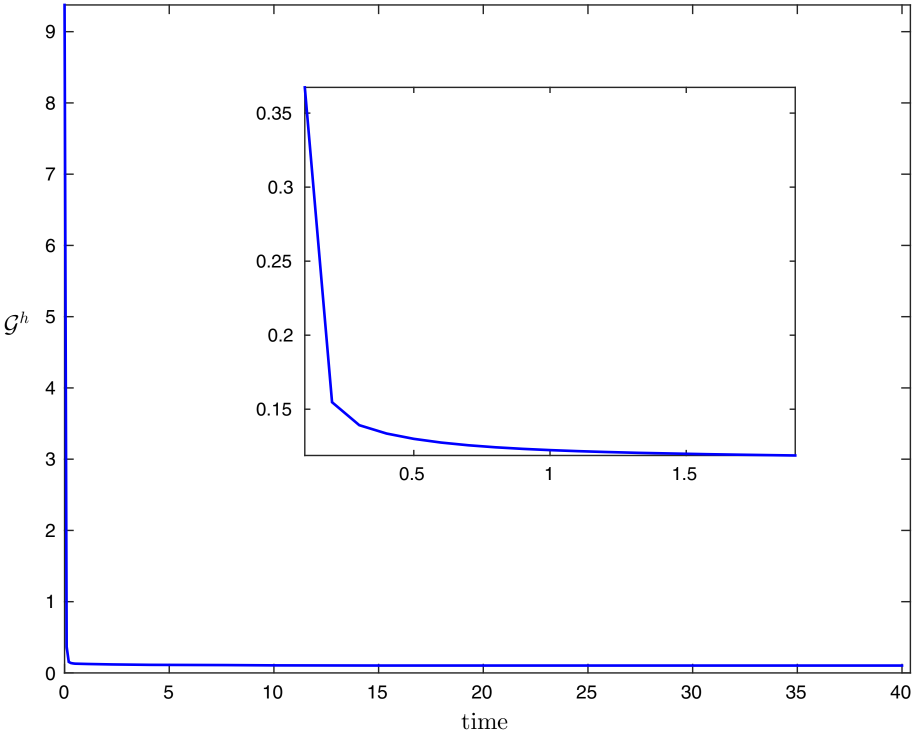

Fig. 17 Energy evolution obtained by the stabilized semi-implicit Lorentz gauge scheme (2.33)–(2.34) with $\Delta t = 0.1$ and $h = \frac{1}{64}$ for Example 5.2 with $H = 5$

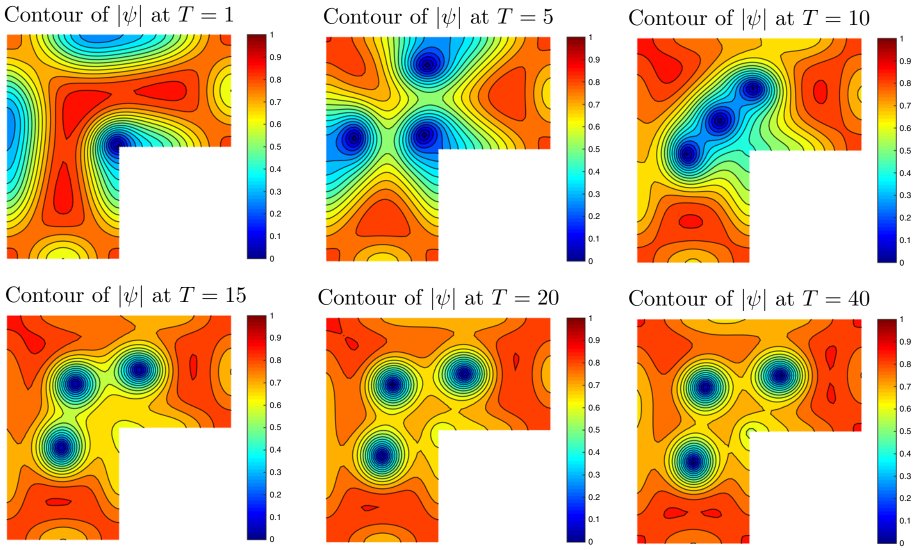

Fig. 18 Plots of the contour of simulated $|\psi|$ at time $T = 1, 5, 15, 20, 20$ and 40 by the Lorentz gauge scheme (2.33)–(2.34) with $\Delta t = 0.1$ and $h = \frac{1}{64}$ for Example 5.2 with $H = 7.2$

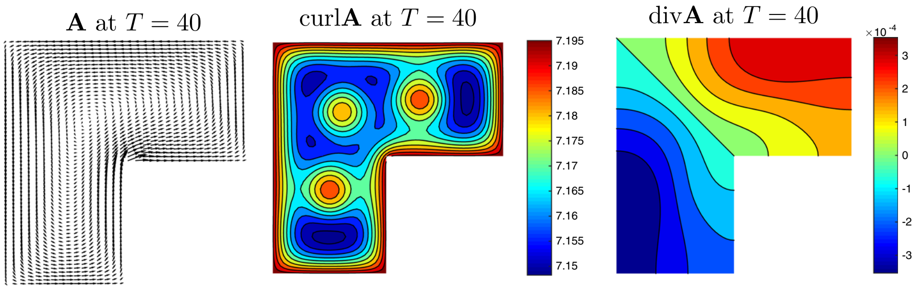

Fig. 19 Plots of simulated $\mathbf{A}$, curl$\mathbf{A}$ and div$\mathbf{A}$ at time $T = 40$ computed by the Lorentz gauge scheme (2.33)–(2.34) with $\Delta t = 0.1$ and $h = \frac{1}{64}$ for Example 5.2 with $H = 7.2$

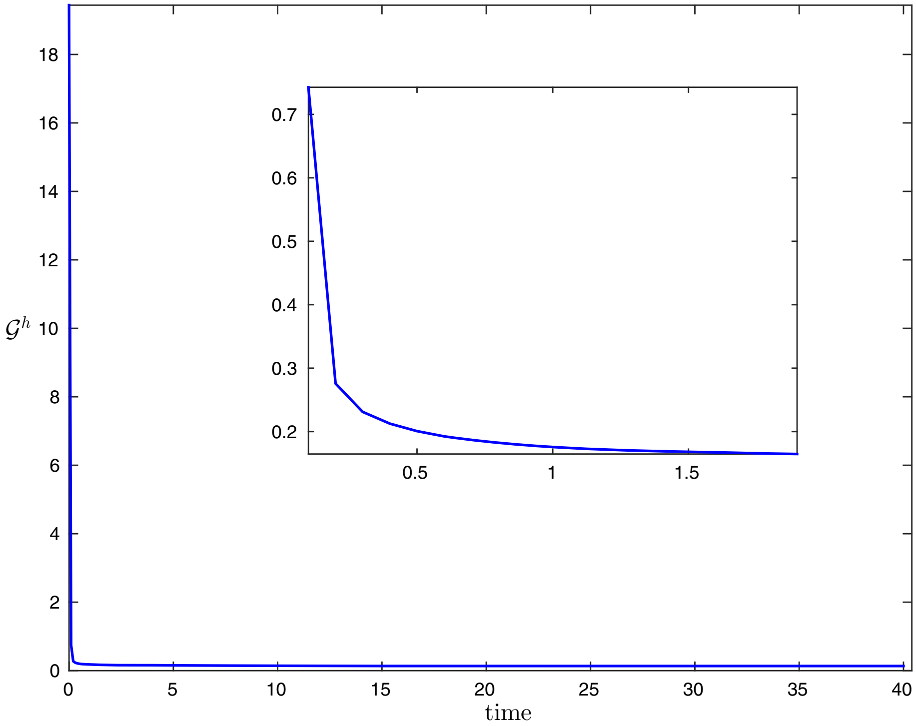

Fig. 20 Energy evolution obtained by the stabilized semi-implicit Lorentz gauge scheme (2.33)–(2.34) with $\Delta t = 0.1$ and $h = \frac{1}{64}$ for Example 5.2 with $H = 7.2$

time, we establish a connection between the gauge-invariant scheme and the lowest order rectangular Nédélec element in space. That is, the widely-used gauge-invariant discretization on a staggered mesh under the zero-electric potential gauge can be viewed a mass-lumped version of Nédélec element approximation, and the Lorentz gauge finite difference scheme as a mass-lumped mixed FEM. Numerical results show that the stabilized semi-implicit gauge-invariant schemes under both zero-electric potential gauge and Lorentz gauge can provide accurate vortex pattern simulations of superconductors on non-convex and multi-connected domains. Although the method considered here is for the two-dimensional superconduc-

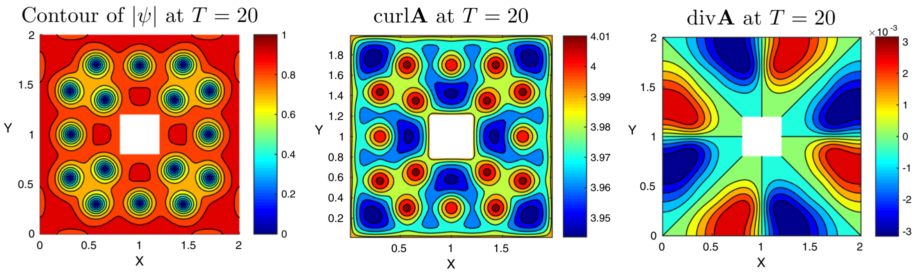

Fig. 21 Plots of the contour of simulated $|\psi|$, curl**A** and div**A** at time $T = 20$ by the stabilized semi-implicit Lorentz gauge scheme (2.33)–(2.34) with $\Delta t = 0.05$ and $h = \frac{1}{80}$

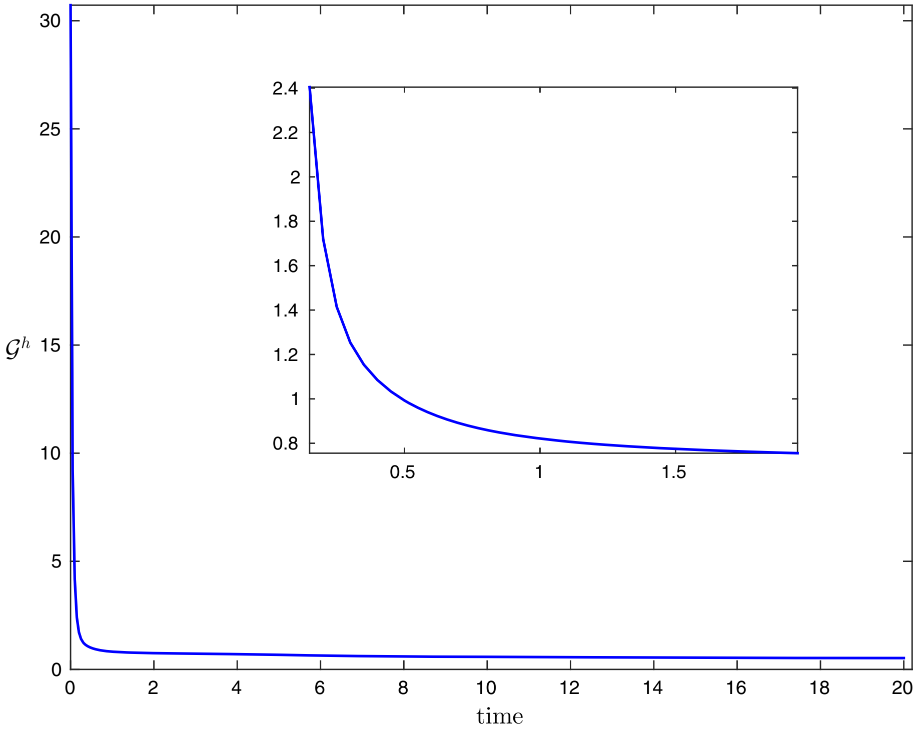

Fig. 22 Energy evolution obtained by the stabilized semi-implicit Lorentz gauge scheme (2.33)–(2.34) with $\Delta t = 0.05$ and $h = \frac{1}{80}$ for Example 5.3

tivity model, our work provides a fundamental understanding of the gauge-invariant finite difference approximation, and we expect to generalize it to the three-dimensional space problems and in more general settings in the future research. Due to the low regularity of the exact solution on non-convex domains and the gauge-invariant approximation, a rigorous error analysis is challenging and desirable, which will also be conducted in our ongoing work.

Appendix

A An Example with Explicit Coefficient Matrices

In this appendix, we provide an example on a 2 × 2 mesh to show the equivalence of the gauge invariant finite difference approximation and the mass-lumped mixed finite element method. To this end, we shall only consider the Lorentz gauge scheme for **A** (2.34) and the mixed FEM (4.8)–(4.9). For simplicity, we take $\Omega = (0, 1)^2$ and set $h = \frac{1}{2}$. There are 9 degrees of freedom (DOFs) for Φ and 12 DOFs for **A**, see Fig. 23.

The Lorentz gauge scheme (2.33)–(2.34) can be written as

$$\frac{1}{\Delta t}\overrightarrow{A}^{n} - \nabla_h D_h \overrightarrow{A}^{n} + \mathbf{K}_1 \overrightarrow{A}^{n} = \mathrm{RHS}, \tag{A.1}$$

where ∇_h is a 12×9 gradient matrix and D_h is a 9×12 divergence matrix defined respectively by

$$\nabla_h = \frac{1}{h}\begin{bmatrix} -1 & 1 & 0 & & & & & & \\ 0 & -1 & 1 & & & & & & \\ -1 & 0 & 0 & 1 & 0 & 0 & & & \\ 0 & -1 & 0 & 0 & 1 & 0 & & & \\ 0 & 0 & -1 & 0 & 0 & 1 & & & \\ & & & -1 & 1 & 0 & & & \\ & & & 0 & -1 & 1 & & & \\ & & & -1 & 0 & 0 & 1 & 0 & 0 \\ & & & 0 & -1 & 0 & 0 & 1 & 0 \\ & & & 0 & 0 & -1 & 0 & 0 & 1 \\ & & & & & & -1 & 1 & 0 \\ & & & & & & 0 & -1 & 1 \end{bmatrix},$$

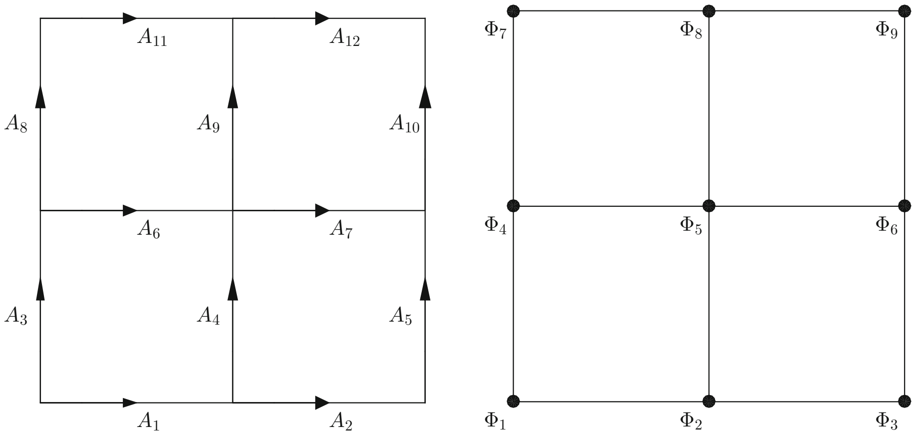

Fig. 23 An illustration of labeled global DOFs for **A** and Φ on a 2 × 2 mesh

$$D_h = \frac{1}{h}\begin{bmatrix} 2 & 0 & 2 & 0 & 0 & & & & & & & \\ -1 & 1 & 0 & 2 & 0 & & & & & & & \\ 0 & -2 & 0 & 0 & 2 & & & & & & & \\ & & -1 & 0 & 0 & 2 & 0 & 1 & 0 & 0 & & \\ & & 0 & -1 & 0 & -1 & 1 & 0 & 1 & 0 & & \\ & & 0 & 0 & -1 & 0 & -2 & 0 & 0 & 1 & & \\ & & & & & & & -2 & 0 & 0 & 2 & 0 \\ & & & & & & & 0 & -2 & 0 & -1 & 1 \\ & & & & & & & 0 & 0 & -2 & 0 & -2 \end{bmatrix},$$

and $\mathbf{K}_1$ is the coefficient matrix defined by

$$\mathbf{K}_1 = \frac{1}{h^2}\begin{bmatrix} 2 & 0 & -2 & 2 & 0 & -2 & 0 & & & & & \\ 0 & 2 & 0 & -2 & 2 & 0 & -2 & & & & & \\ -2 & 0 & 2 & -2 & 0 & 2 & 0 & & & & & \\ 1 & -1 & -1 & 2 & -1 & -1 & 1 & & & & & \\ 0 & 2 & 0 & -2 & 2 & 0 & -2 & & & & & \\ -1 & 0 & 1 & -1 & 0 & 2 & 0 & -1 & 1 & 0 & -1 & 0 \\ 0 & -1 & 0 & 1 & -1 & 0 & 2 & 0 & -1 & 1 & 0 & -1 \\ & & & & & -2 & 0 & 2 & -2 & 0 & 2 & 0 \\ & & & & & 1 & -1 & -1 & 2 & -1 & -1 & 1 \\ & & & & & 0 & 2 & 0 & -2 & 2 & 0 & -2 \\ & & & & & -2 & 0 & 2 & -2 & 0 & 2 & 0 \\ & & & & & 0 & -2 & 0 & 2 & -2 & 0 & 2 \end{bmatrix}.$$

Let us recall that the mixed FEM introduces $\Phi = -\operatorname{div} \mathbf{A}$ as an extra variable. Based on the lowest order bilinear element space S_h and lowest order rectangular Nédélec edge element space V_h, we look for $(\Phi_h^n, \mathbf{A}_h^n) \in S_h \times V_h$ such that

$$(\Phi_h^n, \omega_h) - (\mathbf{A}_h^n, \nabla \omega_h) = 0, \quad \forall\, \omega_h \in S_h, \tag{A.2}$$

$$\frac{1}{\Delta t}(\mathbf{A}_h^n, \mathbf{v}_h) + (\nabla \Phi_h^n, \mathbf{v}_h) + (\mathrm{curl}\mathbf{A}_h^n, \mathrm{curl}\mathbf{v}_h) = \mathrm{RHS}\,, \quad \forall\, \mathbf{v}_h \in V_h, \tag{A.3}$$

which further can be represented by the following matrix equations

$$\mathbf{M}_{\text{bilinear}} \overrightarrow{\Phi}^n - \mathbf{D}_h \overrightarrow{A}^n = 0, \tag{A.4}$$

$$\frac{1}{\Delta t} \boldsymbol{M} \overrightarrow{A}^n + \mathbf{D}_h^T \overrightarrow{\Phi}^n + \mathbf{K}_2 \overrightarrow{A}^n = \mathrm{RHS}\,. \tag{A.5}$$

On the 2×2 mesh, the above mass matrix $\mathbf{M}_{\text{bilinear}}$ generated by the lowest order bilinear Lagrange element space and the matrix $\boldsymbol{D}_h$ are defined by

$$\mathbf{M}_{\text{bilinear}} = h^2 \begin{bmatrix} \frac{1}{9} & \frac{1}{18} & 0 & \frac{1}{18} & \frac{1}{36} & 0 & & & \\ \frac{1}{18} & \frac{2}{9} & \frac{1}{18} & \frac{1}{36} & \frac{1}{9} & \frac{1}{36} & & & \\ 0 & \frac{1}{18} & \frac{1}{9} & 0 & \frac{1}{36} & \frac{1}{18} & & & \\ \frac{1}{18} & \frac{1}{36} & 0 & \frac{2}{9} & \frac{1}{9} & 0 & \frac{1}{18} & \frac{1}{36} & 0 \\ \frac{1}{36} & \frac{1}{9} & \frac{1}{36} & \frac{1}{9} & \frac{4}{9} & \frac{1}{9} & \frac{1}{36} & \frac{1}{9} & \frac{1}{36} \\ 0 & \frac{1}{36} & \frac{1}{18} & 0 & \frac{1}{9} & \frac{2}{9} & 0 & \frac{1}{36} & \frac{1}{18} \\ & & & \frac{1}{18} & \frac{1}{36} & 0 & \frac{1}{9} & \frac{1}{18} & 0 \\ & & & \frac{1}{36} & \frac{1}{9} & \frac{1}{36} & \frac{1}{18} & \frac{2}{9} & \frac{1}{18} \\ & & & 0 & \frac{1}{36} & \frac{1}{18} & 0 & \frac{1}{18} & \frac{1}{9} \end{bmatrix},$$

$$\boldsymbol{D}_h = \begin{bmatrix} -\frac{1}{3} & 0 & -\frac{1}{3} & -\frac{1}{6} & 0 & -\frac{1}{6} & 0 & & & & & \\ \frac{1}{3} & -\frac{1}{3} & -\frac{1}{6} & -\frac{2}{3} & -\frac{1}{6} & \frac{1}{6} & -\frac{1}{6} & & & & & \\ 0 & \frac{1}{3} & 0 & -\frac{1}{6} & -\frac{1}{3} & 0 & \frac{1}{6} & & & & & \\ -\frac{1}{6} & 0 & \frac{1}{3} & \frac{1}{6} & 0 & -\frac{2}{3} & 0 & -\frac{1}{3} & -\frac{1}{6} & 0 & -\frac{1}{6} & 0 \\ \frac{1}{6} & -\frac{1}{6} & \frac{1}{6} & \frac{2}{3} & \frac{1}{6} & \frac{2}{3} & -\frac{2}{3} & -\frac{1}{6} & -\frac{2}{3} & -\frac{1}{6} & \frac{1}{6} & -\frac{1}{6} \\ 0 & \frac{1}{6} & 0 & \frac{1}{6} & \frac{1}{3} & 0 & \frac{2}{3} & 0 & -\frac{1}{6} & -\frac{1}{3} & 0 & \frac{1}{6} \\ & & & & & -\frac{1}{6} & 0 & \frac{1}{3} & \frac{1}{6} & 0 & -\frac{1}{3} & 0 \\ & & & & & \frac{1}{6} & -\frac{1}{6} & \frac{1}{6} & \frac{2}{3} & \frac{1}{6} & \frac{1}{3} & -\frac{1}{3} \\ & & & & & 0 & \frac{1}{6} & 0 & \frac{1}{6} & \frac{1}{3} & 0 & \frac{1}{3} \end{bmatrix},$$

and the mass matrix $\mathbf{M}$ and stiffness matrix $\mathbf{K}_2$ generated by the lowest order rectangular Nédélec edge element space are defined respectively by

$$\mathbf{M} = h^2 \begin{bmatrix} \frac{1}{3} & 0 & & & & \frac{1}{6} & 0 & & & & & \\ 0 & \frac{1}{3} & & & & 0 & \frac{1}{6} & & & & & \\ & & \frac{1}{3} & \frac{1}{6} & 0 & & & & & & & \\ & & \frac{1}{6} & \frac{2}{3} & \frac{1}{6} & & & & & & & \\ & & 0 & \frac{1}{6} & \frac{1}{3} & & & & & & & \\ \frac{1}{6} & 0 & & & & \frac{2}{3} & 0 & & & & \frac{1}{6} & 0 \\ 0 & \frac{1}{6} & & & & 0 & \frac{2}{3} & & & & 0 & \frac{1}{6} \\ & & & & & & & \frac{1}{3} & \frac{1}{6} & 0 & & \\ & & & & & & & \frac{1}{6} & \frac{2}{3} & \frac{1}{6} & & \\ & & & & & & & 0 & \frac{1}{6} & \frac{1}{3} & & \\ & & & & & \frac{1}{6} & 0 & & & & \frac{1}{3} & 0 \\ & & & & & 0 & \frac{1}{6} & & & & 0 & \frac{1}{3} \end{bmatrix},$$

$$\mathbf{K}_2=\begin{bmatrix}
1 & 0 & -1 & 1 & 0 & -1 & 0 & & & & & \\
0 & 1 & 0 & -1 & 1 & 0 & -1 & & & & & \\
-1 & 0 & 1 & -1 & 0 & 1 & 0 & & & & & \\
1 & -1 & -1 & 2 & -1 & -1 & 1 & & & & & \\
0 & 1 & 0 & -1 & 1 & 0 & -1 & & & & & \\
-1 & 0 & 1 & -1 & 0 & 2 & 0 & -1 & 1 & 0 & -1 & 0 \\
0 & -1 & 0 & 1 & -1 & 0 & 2 & 0 & -1 & 1 & 0 & -1 \\
 & & & & & -1 & 0 & 1 & -1 & 0 & 1 & 0 \\
 & & & & & 1 & -1 & -1 & 2 & -1 & -1 & 1 \\
 & & & & & 0 & 1 & 0 & -1 & 1 & 0 & -1 \\
 & & & & & -1 & 0 & 1 & -1 & 0 & 1 & 0 \\
 & & & & & 0 & -1 & 0 & 1 & -1 & 0 & 1
\end{bmatrix}.$$

If the mass-lumping is used, then it holds

$$(\Phi_h^n, \omega_h)_h - (\mathbf{A}_h^n, \nabla\omega_h)_h = 0, \tag{A.6}$$

$$\frac{1}{\Delta t}(\mathbf{A}_h^n, \mathbf{v}_h)_h + (\nabla\Phi_h^n, \mathbf{v}_h)_h + (\mathrm{curl}\mathbf{A}_h^n, \mathrm{curl}\mathbf{v}_h) = \mathrm{RHS}\,, \tag{A.7}$$

and we can obtain the following matrix equations

$$\widetilde{\mathbf{M}}_{\text{bilinear}}\overrightarrow{\Phi}^n - \widetilde{\mathbf{D}}_h\overrightarrow{A}^n = 0\,, \tag{A.8}$$

$$\frac{1}{\Delta t}\widetilde{\mathbf{M}}\overrightarrow{A}^n + \widetilde{\mathbf{D}}_h^T\overrightarrow{\Phi}^n + \mathbf{K}_2\overrightarrow{A}^n = \mathrm{RHS}\,, \tag{A.9}$$

where $\widetilde{\mathbf{M}}_{\text{bilinear}}$ and $\widetilde{\boldsymbol{M}}$ are diagonal matrices as

$$\widetilde{\mathbf{M}}_{\text{bilinear}} = \mathrm{diag}\left(\left[\,\tfrac14\ \tfrac12\ \tfrac14\ \tfrac12\ 1\ \tfrac12\ \tfrac14\ \tfrac12\ \tfrac14\,\right]^T\right),$$

$$\widetilde{\boldsymbol{M}} = \mathrm{diag}\left(\left[\,\tfrac12\ \tfrac12\ \tfrac12\ 1\ \tfrac12\ 1\ 1\ \tfrac12\ 1\ \tfrac12\ \tfrac12\ \tfrac12\,\right]^T\right),$$

and

$$\widetilde{\mathbf{D}}_h = h\begin{bmatrix}
-\frac12 & 0 & -\frac12 & 0 & 0 & & & & & & & \\
\frac12 & -\frac12 & 0 & -1 & 0 & & & & & & & \\
0 & \frac12 & 0 & 0 & -\frac12 & & & & & & & \\
 & & \frac12 & 0 & 0 & -1 & 0 & -\frac12 & 0 & 0 & & \\
 & & 0 & 1 & 0 & 1 & -1 & 0 & -1 & 0 & & \\
 & & 0 & 0 & \frac12 & 0 & 1 & 0 & 0 & -\frac12 & & \\
 & & & & & & & \frac12 & 0 & 0 & -\frac12 & 0 \\
 & & & & & & & 0 & 1 & 0 & \frac12 & -\frac12 \\
 & & & & & & & 0 & 0 & \frac12 & 0 & \frac12
\end{bmatrix}.$$

By taking matrices $\widetilde{\mathbf{M}}_{\text{bilinear}}$, $\widetilde{\boldsymbol{M}}$ and $\widetilde{\mathbf{D}}_h$ into (A.9), we can deduce that

$$\frac{1}{\Delta t}\overrightarrow{A}^n + \widetilde{\mathbf{M}}^{-1}\widetilde{\mathbf{D}}_h^T\widetilde{\mathbf{M}}_{\text{bilinear}}^{-1}\widetilde{\mathbf{D}}_h\overrightarrow{A}^n + \widetilde{\mathbf{M}}^{-1}\mathbf{K}_2\overrightarrow{A}^n = \mathrm{RHS}\,.$$

It is easy to verify the following matrix qualities

$$\nabla_h = \widetilde{\mathbf{M}}^{-1}\widetilde{\mathbf{D}}_h^T, \quad -D_h = \widetilde{\mathbf{M}}_{\text{bilinear}}^{-1}\widetilde{\mathbf{D}}_h, \quad \mathbf{K}_1 = \widetilde{\mathbf{M}}^{-1}\mathbf{K}_2,$$

which confirm our observation. Finally, we shall point out that similar equivalences also hold for L-shape and multi-connected domains.

References

1. Alstrom, T., Sorensen, M., Pedersen, N., Madsen, S.: Magnetic flux lines in complex geometry type-II superconductors studied by the time dependent Ginzburg–Landau equation. Acta Appl. Math. **115**, 63–74 (2011)
2. Arnold, D., Falk, R., Winther, R.: Finite element exterior calculus: from Hodge theory to numerical stability. Bull. Am. Math. Soc. (N.S.) **47**, 281–354 (2010)
3. Buscaglia, G., Bolech, C., Lopez, A.: On the numerical solution of the time-dependent Ginzburg–Landau equations in multiply connected domains. In: Berger, J., Rubinstein, J. (eds.) Connectivity and superconductivity. LNP m62, pp. 200–214. Springer, Berlin (2000)
4. Carey, G., Knezevic, D.: Multiscale and hysteresis effects in vortex pattern simulations for Ginzburg–Landau problems. Int. J. Numer. Meth. Eng. **81**, 866–891 (2010)
5. Chapman, S.J., Howison, S.D., Ockendon, J.R.: Macroscopic models for superconductivity. SIAM Rev. **34**, 529–560 (1992)
6. Chen, Z.: Mixed finite element methods for a dynamical Ginzburg–Landau model in superconductivity. Numer. Math. **76**, 323–353 (1997)
7. Chen, Z., Hoffmann, K.: Numerical studies of a non-stationary Ginzburg–Landau model for superconductivity. Adv. Math. Sci. Appl. **5**, 363–389 (1995)
8. Christiansen, S., Halvorsen, T.: A Gauge invariant discretization on simplicial grids of the Schrödinger eigenvalue problem in an electromagnetic field. SIAM J. Numer. Anal. **49**, 331–345 (2011)
9. Coskun, E., Kwong, M.: Simulating vortex motion in superconducting films with the time-dependent Ginzburg–Landau equations. Nonlinearity **10**, 579–593 (1997)
10. Du, Q.: Finite element methods for the time-dependent Ginzburg–Landau model of superconductivity. Comput. Math. Appl. **27**, 119–133 (1994)
11. Du, Q.: Discrete gauge-invariant approximations of a time dependent Ginzburg–Landau model of superconductivity. Math. Comput. **67**, 965–986 (1998)
12. Du, Q., Gunzburger, M.D., Peterson, J.S.: Analysis and approximation of the Ginzburg–Landau model of superconductivity. SIAM Rev. **34**, 54–81 (1992)
13. Du, Q., Ju, L., Li, X., Qiao, Z.: Stabilized linear semi-implicit schemes for the nonlocal Cahn–Hilliard equation. J. Comput. Phys. **363**, 39–54 (2018)
14. Du, Q., Nicolaides, R., Wu, X.: Analysis and convergence of a covolume approximation of the Ginzburg–Landau model of superconductivity. SIAM J. Numer. Anal. **35**, 1049–1072 (1998)
15. Frahm, H., Ullah, S., Dorsey, A.: Flux dynamics and the growth of the superconducting phase. Phys. Rev. Lett. **66**, 3067–3070 (1991)
16. Gao, H., Li, B., Sun, W.: Optimal error estimates of linearized Crank–Nicolson Galerkin FEMs for the time-dependent Ginzburg–Landau equations in superconductivity. SIAM J. Numer. Anal. **52**, 1183–1202 (2014)
17. Gao, H., Sun, W.: An efficient fully linearized semi-implicit Galerkin-mixed FEM for the dynamical Ginzburg–Landau equations of superconductivity. J. Comput. Phys. **294**, 329–345 (2015)
18. Gao, H., Sun, W.: A new mixed formulation and efficient numerical solution of Ginzburg–Landau equations under the temporal gauge. SIAM J. Sci. Comput. **38**, A1339–A1357 (2016)
19. Gao, H., Sun, W.: Analysis of linearized Galerkin—mixed FEMs for the time-dependent Ginzburg–Landau equations of superconductivity. Adv. Comput. Math. **44**, 923–949 (2018)
20. Gor'kov, L.P., Eliashberg, G.M.: Generalization of the Ginzburg–Landau equations for non-stationary problems in the case of alloys with paramagnetic impurities. Sov. Phys. JETP **27**, 328–334 (1968)
21. Gropp, W., Kaper, H., Leaf, G., Levine, D., Palumbo, M., Vinokur, V.: Numerical simulation of vortex dynamics in type-II superconductors. J. Comput. Phys. **123**, 254–266 (1996)
22. Gunter, D., Kaper, H., Leaf, G.: Implicit integration of the time-dependent Ginzburg–Landau equations of superconductivity. SIAM J. Sci. Comput. **23**, 1943–1958 (2002)
23. Kato, R., Enomoto, Y., Maekawa, S.: Computer simulations of dynamics of flux lines in type-II superconductors. Phys. Rev. B **47**, 8016–8024 (1993)

24. Kaper, H., Kwong, M.: Vortex configurations in type-II superconducting films. J. Comput. Phys. **119**, 120–131 (1995)
25. Kim, S., Burkardt, J., Gunzburger, M., Peterson, J., Hu, C.: Effects of sample geometry on the dynamics and configurations of vortices in mesoscopic superconductors. Phys. Rev. B **76**, 024509 (2007)
26. Li, B.: Convergence of a decoupled mixed FEM for the dynamic Ginzburg-Landau equations in nonsmooth domains with incompatible initial data. Calcolo **54**, 1441–1480 (2017)
27. Li, B., Zhang, Z.: Mathematical and numerical analysis of time-dependent Ginzburg–Landau equations in non-convex polygons based on Hodge decomposition. Math. Comput. **86**, 1579–1608 (2017)
28. Li, B., Zhang, Z.: A new approach for numerical simulation of the time-dependent Ginzburg–Landau equations. J. Comput. Phys. **303**, 238–250 (2015)
29. Liao, H., Zhou, S., Shi, X.: Simulating the time-dependent Ginzburg–Landau equations for type-II superconductors by finite-difference method. Chin. Phys. **13**, 0737-09 (2004)
30. Monk, P.: Finite Element Methods for Maxwell's Equations. Oxford University Press, New York (2003)
31. Mu, M.: A linearized Crank–Nicolson–Galerkin method for the Ginzburg–Landau model. SIAM J. Sci. Comput. **18**, 1028–1039 (1997)
32. Mu, M., Huang, Y.: An alternating Crank–Nicolson method for decoupling the Ginzburg–Landau equations. SIAM J. Numer. Anal. **35**, 1740–1761 (1998)
33. Raza, N., Sial, S., Siddiqi, S.: Approximating time evolution related to Ginzburg–Landau functionals via Sobolev gradient methods in a finite-element setting. J. Comput. Phys. **229**, 1621–1625 (2010)
34. Richardson, W., Pardhanani, A., Carey, G., Ardelea, A.: Numerical effects in the simulation of Ginzburg–Landau models for superconductivity. Int. J. Numer. Meth. Eng. **59**, 1251–1272 (2004)
35. Stosic, Darko, Stosic, Dusan, Ludermir, T., Stosic, B., Milosevic, M.: GPU-advanced 3D electromagnetic simulations of superconductors in the Ginzburg–Landau formalism. J. Comput. Phys. **322**, 183–198 (2016)
36. Thomée, V.: Galerkin Finite Element Methods for Parabolic Problems. Springer, Berlin (1997)
37. Tinkham, M.: Introduction to Superconductivity. McGraw-Hill, New York (1975)
38. Xu, C., Tang, T.: Stability analysis of large time-stepping methods for epitaxial growth models. SIAM J. Numer. Anal. **44**, 1759–1779 (2006)